

---

# Towards a clinically accessible radiology foundation model: open-access and lightweight, with automated evaluation

---

Juan Manuel Zambrano Chaves<sup>3◊\*</sup> Shih-Cheng Huang<sup>3◊\*</sup>,  
Yanbo Xu<sup>1\*</sup>, Hanwen Xu<sup>2\*</sup>, Naoto Usuyama<sup>1\*</sup>, Sheng Zhang<sup>1\*</sup>,

Fei Wang<sup>4</sup>, Yujia Xie<sup>1</sup>, Mahmoud Khademi<sup>1</sup>, Ziyi Yang<sup>1</sup>, Hany Awadalla<sup>1</sup>,  
Julia Gong<sup>1</sup>, Houdong Hu<sup>1</sup>, Jianwei Yang<sup>1</sup>, Chunyuan Li<sup>1</sup>, Jianfeng Gao<sup>1</sup>,  
Yu Gu<sup>1</sup>, Cliff Wong<sup>1</sup>, Mu Wei<sup>1</sup>, Tristan Naumann<sup>1</sup>, Muhao Chen<sup>5</sup>,  
Matthew P. Lungren<sup>1,3,6</sup>, Serena Yeung-Levy<sup>3</sup>, Curtis P. Langlotz<sup>3</sup>,  
Sheng Wang<sup>2,‡</sup>, Hoifung Poon<sup>1,‡</sup>

<sup>1</sup>Microsoft Research    <sup>2</sup>University of Washington    <sup>3</sup>Stanford University

<sup>4</sup>University of Southern California    <sup>5</sup>University of California, Davis

<sup>6</sup>University of California, San Francisco

## Abstract

The scaling laws and extraordinary performance of large foundation models motivate the development and utilization of such models in biomedicine. However, despite early promising results on some biomedical benchmarks, there are still major challenges that need to be addressed before these models can be used in real-world clinics. Frontier general-domain models such as GPT-4V still have significant performance gaps in multimodal biomedical applications. More importantly, less-acknowledged pragmatic issues, including accessibility, model cost, and tedious manual evaluation make it hard for clinicians to use state-of-the-art large models directly on private patient data. Here, we explore training open-source small multimodal models (SMMs) to bridge competency gaps for unmet clinical needs in radiology. To maximize data efficiency, we adopt a modular approach by incorporating state-of-the-art pre-trained models for image and text modalities, and focusing on training a lightweight adapter to ground each modality to the text embedding space, as exemplified by LLaVA-Med. For training, we assemble a large dataset of over 697 thousand radiology image-text pairs. For evaluation, we propose CheXprompt, a GPT-4-based metric for factuality evaluation, and demonstrate its parity with expert evaluation. For best practice, we conduct a systematic ablation study on various choices in data engineering and multimodal training. The resulting LLaVA-Rad (7B) model attains state-of-the-art results on standard radiology tasks such as report generation and cross-modal retrieval, even outperforming much larger models such as GPT-4V and Med-PaLM M (84B). Moreover, LLaVA-Rad requires only one day to be trained on over 697 thousand image-text pairs using a standard 8-A100 GPU cluster, allowing further fine-tuning by clinicians using their own data. The inference of LLaVA-Rad is fast and can be performed on a single V100 GPU in private settings, offering a promising state-of-the-art tool for real-world clinical applications.

---

\* Equal Contribution. ◊ Work performed as an intern at Microsoft Research. ‡ Corresponding authors: swang@cs.washington.edu, hoifung@microsoft.com.

## Introduction

Foundation models, trained on massive amounts of unlabelled data using self-supervised learning, enable rapid adaptation to various downstream tasks with minimal requirement for task-specific labeled data [5, 36]. Due to the high cost of annotating biomedical data [22, 21], foundation models are poised to become a new paradigm in biomedicine, achieving state-of-the-art results on many applications, including medical question answering [47, 36] and medical image classification [4, 3]. Recently, multimodal generative AI has emerged as an exciting frontier in the biomedical domain, expanding the application scope from single-modality to multi-modality (e.g., text and image), such as visual question answering and radiology report generation [29, 47, 44]. While existing models are still largely evaluated on artificial biomedical benchmarks, their promising performance demonstrates their potential in clinical applications.

However, there are still major bottlenecks hindering the progress toward using foundation models in real-world clinical settings. First, sharing patient data with large foundation models hosted on the cloud is subject to privacy concerns [45]. Therefore, clinicians may prefer to run inference and fine-tuning locally. Second, existing state-of-the-art models are often very large and resource-intensive, which makes local deployment challenging. Smaller models incur smaller carbon footprint [46] and offer reduced serving costs and latency, which is of particular importance in resource-constrained settings outside of data centers [51]. However, while small language models have shown success in text domains [16, 34, 28], small multimodal models still have significant performance gaps compared to larger models [47, 44]. Third, many state-of-the-art models are inaccessible [51], necessitating the development of effective open-source models for biomedicine. Finally, even the best models are still subject to errors such as hallucination and there exist limited methods to reliably verify the correctness of model outputs at scale, especially in the specialized field of biomedicine [10].

To bridge this gap between existing medical foundation models and real-world clinical applications, we have developed LLaVA-Rad, a small multimodal model (SMM) that attains state-of-the-art performance in standard radiology imaging tasks (**Fig. 1**). We focus our study on identifying key findings from chest X-ray (CXR) images, the most commonly performed medical imaging examination. Automatically drafting high-quality radiology reports is a challenging but clinically meaningful task that could directly increase radiologist productivity and potentially improve communication and decrease burnout [27]. Existing frontier models such as GPT-4V still have a large performance gap even on such a fundamental medical application. To develop LLaVA-Rad, we adopt a modular approach by incorporating state-of-the-art open-source pretrained models for image and text modalities, and focusing on training a lightweight adapter to ground each modality to the text embedding space, as exemplified by LLaVA-Med [29].

For training, we assemble a large dataset comprising 697,435 radiology image-report pairs from 7 diverse sources. Some data sources only contain structured labels of key findings, in which case we use GPT-4 to synthesize the report based on the ground-truth labels. We only apply this GPT-4 synthesis to the training data.

For evaluation, we report standard metrics such as  $n$ -gram-based BLEU and ROUGE, as well as factuality checks based on CheXpert and RadGraph [43, 25]. Additionally, we propose CheXprompt, a factuality evaluation method based on GPT-4. Compared to existing automatic metrics, we show that CheXprompt is more consistent with error quantification by practicing radiologists, thus demonstrating the potential of using GPT-4 for evaluation in a manner that is both scalable and highly relevant to medical practice.

To establish best practices for biomedical multimodal learning, we conduct a systematic ablation study on various choices in data engineering and multimodal training. The resulting LLaVA-Rad (7B) model attains state-of-the-art results on standard radiology tasks such as report generation and cross-modal retrieval, even outperforming much larger models such as GPT-4V and Med-PaLM M (84B) [47].

LLaVA-Rad inference is fast and can be run on a single V100 GPU in private settings, offering a promising state-of-the-art tool for real-world clinical applications. In addition, LLaVA-Rad training is also very efficient, taking just one day on over 697 thousand image-text pairs using a standard 8-A100 cluster. This means that clinicians can further efficiently fine-tune the model as needed using their private data. By examining the model weights, we found that LLaVA-Rad can ground key

regions of abnormalities to generated words in the output report, which signifies future opportunities to synergize with latest progress in biomedical segmentation and grounded report generation.

In summary, we develop LLaVA-Rad, a lightweight yet high-performing radiology multimodal model for clinical applications. The promising performance of LLaVA-Rad shows that its underlying modular approach can effectively and efficiently bridge the multimodal performance gap in existing frontier models, enabling clinical access with limited computational resources.

## Results

### Overview of LLaVA-Rad

LLaVA-Rad represents an emerging paradigm in exploring small multimodal models (SMMs), following the proliferation of small language models (SLMs) (**Fig. 1**). Despite its compact size, which is over an order of magnitude smaller than prior state-of-the-art models such as Med-PaLM M, LLaVA-Rad attains state-of-the-art performance on standard radiology tasks. This bodes well for potential clinical applications with limited computational resources.

Our intuition for designing LLaVA-Rad is that a lightweight, specialized SMM can be efficiently developed by decomposing training into unimodal pretraining on individual modalities followed by lightweight cross-modal learning focusing on a small adapter to ground a non-text modality to the text embedding space. For training, we collect 697 thousand pairs of fully de-identified CXR images and associated radiology reports from 7 diverse datasets [24, 41, 14, 37, 17, 26, 6]. These de-identified image-text pairs were sourced from approximately 258,639 patients. The diversity of this data facilitates the pretraining of robust unimodal models (image encoder in this case) and cross-modal adapters (grounding image to text).

LLaVA-Rad can generate radiology report findings given a CXR image. Its training comprises three stages: a pre-training stage, an alignment stage, and a fine-tuning stage. In the first stage of pre-training, we train a domain-specific vision encoder by using 697 thousand pairs of CXR images and associated radiology reports. Since CXR images are often published with a limited number of associated findings or image labels instead of a complete report, we used GPT-4 to synthesize a report based on annotated image labels. Alternatively, reports may be available in other languages, such as the PadChest reports which are available in Spanish, for which we leverage GPT-4 to translate them into English. We also exploit GPT-4 to extract findings from reports when the finding section cannot be reliably extracted using existing rule-based heuristics [26]. These diverse datasets offer us a robust and effective vision encoder for embedding CXR images with the consideration of the associated radiology reports. In the second stage of alignment, we align this pre-trained vision encoder with radiology report findings by training a conditional generative model that generates findings given an input CXR. In this alignment stage, we provide only the CXR as the input, without any associated contexts such as clinical instructions or patient information. As noted by other works [30, 29] and also demonstrated by our ablation studies, this strategy can substantially improve the alignment by forcing the decoder model to focus on the image alone. In the third stage, we fine-tune the model to generate the findings given both the indication for the exam and the image, more closely reflecting the real-world setting. LLaVA-Rad exploits an efficient technique LoRA [19] for fine-tuning, thus substantially reducing the computational time required for this stage. We further reduce the computational time by only using MIMIC-CXR training data instead of the entire 697 thousand image-text pairs in the second and third stages, since reports in MIMIC-CXR are of higher quality. The three stages of LLaVA-Rad can be finished in 8 hours, 4 hours, and 16 hours respectively using 8 A100 GPUs.

### Evaluating LLaVA-Rad using existing report generation benchmarks

We first evaluated LLaVA-Rad on the widely-used radiology report generation benchmark MIMIC-CXR (**Fig. 2, Supplementary Figure 1**) using metrics assessing lexical similarity and factual accuracy. In particular, lexical similarity metrics, such as BLEU and ROUGE, are used in traditional NLP to assess the model’s ability to produce contextually and stylistically aligned output. On the other hand, factual accuracy metrics, including CheXbert-based and RadGraph-based F1 scores [43, 25] are more clinically relevant because they gauge the extent to which the generated reports accurately reflect imaging findings. A high-quality radiology report necessitates both coherence and factual

accuracy, underscoring the importance of evaluating these two types of metrics to ensure the report is both intelligible and clinically precise. Any inaccuracies in the report can potentially lead to adverse patient outcomes, emphasizing the critical need for factual correctness.

We found that LLaVA-Rad achieved superior performance on both groups of metrics (**Fig. 2A-D**). When compared to other models of equivalent size (7B parameters), such as LLaVA-Med [29], CheX-agent [8] and MAIRA-1 [23], LLaVA-Rad demonstrates significant advancements in performance across all evaluated metrics. Furthermore, LLaVA-Rad is more efficient than the current overall leading model, Med-PaLM M [47], with an order of magnitude fewer parameters. This efficiency does not come at the cost of effectiveness; LLaVA-Rad outperforms Med-PaLM M in the most important existing lexical similarity and factual correctness metrics for radiology text (ROUGE-L and F1-RadGraph [54]). A more detailed evaluation (**Supplementary Table 1**) shows that Med-PaLM M marginally surpasses LLaVA-Rad by F1-5 CheXbert metrics, which assess only a small subset of 5 potential abnormalities, and the performance gap is minimal. Most of these competing models also use MIMIC-CXR for training (with the notable exception of LLaVA-Med). We attribute the promising performance of LLaVA-Rad to its modular design, which is more data efficient. The efficiency and the high degree of factual and lexical precision of LLaVA-Rad demonstrate its potential in real-world applications where large models are computationally too costly.

The results of our evaluations reveal that LLaVA-Rad’s superior performance is consistent across other datasets, including CheXpert [24] and Open-I [12]. Notably, CheXpert was used solely for pretraining the image encoder, while Open-I was entirely new to the model, underscoring its robustness and adaptability. Similar to the evaluation on MIMIC, We also employ CheXbert-14, F1-RadGraph, and ROUGE-L to assess the factual accuracy and lexical similarity of the reports on these datasets. As illustrated in **Fig. 3**, LLaVA-Rad significantly outperforms LLaVA-Med, LLaVA, and GPT-4V across all metrics on these datasets.

Finally, to verify the effectiveness of our idea in generating aligned vision and language representations, we examined the learned image encoder in LLaVA-Rad by comparing the performance of using it for retrieval against the image encoders from LLaVA and LLaVA-Med. We observed that LLaVA-Rad attained the best results on both image-to-text and text-to-image retrieval, indicating the high quality of its image encoder by training on 697 thousand text-image pairs (**Fig. 2E**). Moreover, LLaVA-Med performed better than LLaVA, suggesting that better performance can be gained as increasing domain specialization is performed.

### Evaluating LLaVA-Rad using CheXprompt, a GPT-4-based evaluation system

It is well known that existing ngram-based automated report evaluation methods might be biased to pre-defined conditions and have limited correlation with expert assessments [52]. We thus explore the utility of an LLM-based evaluation system, which has shown success in other domains [32, 48, 15]. Specifically, we employ GPT-4 as an evaluator to count how often the generated report commits errors in each of the following six categories, as per a previous study [52]: false positive finding, omission of finding, incorrect location/position of finding, incorrect severity of finding, mention of comparison that is not present in the reference report, omission of comparison describing a change from a previous study. For each error type, we further instruct GPT-4 to distinguish clinically significant and clinically insignificant errors.

We first assessed the rigor of CheXprompt by examining its consistency with expert scoring. To this end, we exploited the ReXval dataset [53], which contains annotations from 6 board certified radiologists on 200 pairs of ground-truth reports from MIMIC-CXR and AI-generated reports. Each radiologist annotates the aforementioned errors in the generated report, also discriminating between clinically significant and insignificant errors. We found that GPT-4-based evaluations were highly correlated with expert scoring by achieving Kendall’s Tau-b correlations greater than 0.75 for total errors and greater than 0.70 for clinically significant errors (**Fig. 4B**). In contrast, none of the existing preferred metrics (ROUGE-L metric, RadGraph-F1, and RadCliQ) obtained a correlation greater than 0.57. Moreover, we found that a similar evaluation system using GPT-3.5Turbo, a less capable model compared to GPT-4, attains a much lower association with expert scoring due to an overestimation of the number of total and clinically significant errors, demonstrating the difficulty of automatically scoring radiology reports.

We also perform a head-to-head comparison of the calculation of total errors as determined by GPT-4Turbo with manual expert ratings in a leave-one-rater-out fashion. **Fig. 4A** summarizes the results of this comparison, which on average shows a mean absolute difference (MAD) of 0.71 between the left-out rater and the average of the remaining ones, whereas GPT-4T has on average 0.55 MAD. We find that the MAD between GPT-4T CheXprompt score and the left-in expert average is smaller compared to the left-out expert in 3 out of 6 cases ( $P < 0.001$ ), slightly larger in 2 out of 6 cases ( $P < 0.001$ ), and not significantly different ( $P > 0.05$ ) in the remaining one case. Altogether, we find that GPT-4T is indistinguishable from expert raters in calculating the total number of errors, increasing our confidence in using this proposed automated metric as a new evaluation method that directly aligns with expert opinions.

After assuring the effectiveness of the GPT-based metric, we evaluated the performance of LLaVA-Rad on the held-out MIMIC-CXR test set using CheXprompt (**Fig. 4C,D**). Similar to our observation using existing metrics, LLaVA-Rad outperforms publicly available report generation models, generating fewer clinically significant and total errors compared to GPT-4V and CheXagent. Moreover, by comparing models within the LLaVA family (e.g., LLaVA-Rad, LLaVA-Med, LLaVA), we observed that fewer errors are made in the generated reports as increasing domain specialization is performed. In particular, LLaVA-Rad generates fewer errors than LLaVA-Med, a LLaVA model tailored to medicine, and LLaVA-Med generates fewer errors than the general-domain model LLaVA. This suggests a trade-off between domain-specific performance and broad applicability, supporting our intuition of developing LLaVA-Rad by continue-pretraining a general model using large amounts of domain-specific data. Finally, to determine the clinical utility of LLaVA-Rad, we explore using the percentage of error-free reports to track the overall performance of report-generation models. A higher percentage of error-free reports increases the utility of a report generation model, given that it directly reflects the number of reports that require little to no radiologist modification following automated generation. Notably, LLaVA-Rad has the highest percentage of error-free reports, with 6.79% reports free of clinically significant errors, and 2.58% free of errors. The same trend was observed in the external validation datasets (CheXpert and Open-I), where LLaVA-Rad demonstrated fewer clinically significant and total errors (**Fig. 3**), with up to 26% error-free reports. While there remains undoubtedly significant growth space, this direction and latest progress are promising.

### Analyzing components of LLaVA-Rad using ablation and case studies

Conducting thorough ablation studies for LLMs is often intractable due to the costly training of multiple variants. In contrast, the small size of LLaVA-Rad enables us to efficiently conduct ablation studies that explain the promising performance of LLaVA-Rad and potentially help derisk design choices for larger models. We compared LLaVA-Rad with 8 variants described in **Supplementary Table 2**. In **Fig. 5A,B**, we investigate two key technical ideas used in LLaVA-Rad: the effect of pre-training a domain-specific image encoder using 697 thousand diverse CXR image-text pairs and the effect of using GPT-4 to augment and organize the data. First, to understand the effect of pre-training an image encoder, we compare LLaVA-Rad with three increasingly domain-specific variants: an image encoder from OpenAI CLIP, an image encoder using BiomedCLIP, and an image encoder from BiomedCLIP but continually pre-trained using MIMIC-CXR only. To avoid data contamination, we only used the training split of MIMIC-CXR. We did not find noticeable overlap between MIMIC-CXR training split and the PubMed data used to pre-train BiomedCLIP. We found that the MIMIC-CXR-based image encoder outperforms the other two variants, indicating the effectiveness of training a domain-specific image encoder. BiomedCLIP-CXR outperforms the BiomedCLIP image encoder continue-pretrained only on MIMIC-CXR (BiomedCLIP-MIMIC-CXR), illustrating the advantage in pre-training using more diverse CXR datasets. Second, we studied the effect of using GPT-4 to process and augment the MIMIC-CXR report data. **Supplementary Table 3** summarizes the data that LLaVA-Rad uses for training in the second and the third stages. It is a combination of rule-based and GPT-structured data. We compare LLaVA-Rad with a variant that only uses rule-based data and a variant that only uses GPT-structured data. We found that LLaVA-Rad attains a better performance than both variants, indicating the effectiveness of GPT-4 data augmentation. The variant that only uses GPT-structured data outperforms the one that only uses rule-based data on factual accuracy metrics, confirming the effectiveness of GPT-4-based structuring in generating clinically precise reports. Finally, it is expected that rule-based variant outperforms GPT-structured variant on n-gram lexical metrics, because the test data is also from rule-based data. These ablation studies support our

intuition that domain-specific data can help us build a small but effective domain-specific model, and help inform best practice in training larger models.

We also investigate how LLaVA-Rad’s attention map on the input image correlates with a given generated word in the report (**Fig. 5C**), which demonstrates the model’s ability to focus on relevant image regions for the generation. A detailed examination reveals a significant variability in attention across different layers and attention heads, with different configurations gravitating towards distinct regions of the image (**Supplementary Figures 2, 3, 4, 5, 6**). Our evaluation also identifies that the aggregation of attention, particularly through averaging the outputs of all heads within the 20th layer, generally yields the most coherent and relevant focal points across a wide array of scenarios. However, this approach does not uniformly apply, as deviations in alignment were observed in certain instances. Conversely, an alternative strategy of taking the maximum across all layers, coupled with an average across heads, demonstrates a consistently high correlation with pertinent image regions. Our proposed attention visualization indicates a strong alignment between the model’s attention and the specific image regions relevant to the generated words. This alignment underscores the model’s efficacy in synthesizing contextual information from visual cues to ground its linguistic output.

## Discussion

To address the significant challenges of developing foundation models for real-world clinical settings, our work introduces LLaVA-Rad, a lightweight radiology small multimodal model (SMM) that offers open-source accessibility while attaining new state-of-the-art results in the domain of radiology report generation. By curating a dataset of 697 thousand CXR images paired with radiology reports from diverse sources, using GPT-4 for dataset processing, coupled with a modular three-stage curriculum training method, we have developed a model that outperforms its larger counterparts, such as GPT-4V and Med-PaLM M, and demonstrates exceptional proficiency in generating accurate and lexically similar radiology reports on the evaluation datasets. Through our attention visualization techniques, LLaVA-Rad offers deep insights into how it prioritizes key regions in chest X-rays, correlating them with specific findings in the generated reports. Furthermore, our utilization of CheXprompt for evaluation demonstrates a closer alignment of automated scoring with expert radiologist assessments than traditional metrics, reinforcing LLaVA-Rad’s superiority in clinical report generation.

The landscape of AI-driven radiology report generation has evolved significantly with the advent of transformers and large multimodal models, ushering in a new era of more sophisticated and accurate models [35, 23, 49, 39, 18, 20, 1]. R2Gen stands out as a pioneering effort in leveraging memory-efficient transformers for report generation [7]. A notable leap forward is CheXagent [8], which leverages an instruction fine-tuned foundation model trained across 28 publicly available datasets, demonstrating an enhanced capability for analyzing and summarizing CXR images. Concurrently, Flamingo-CXR fine-tuned the Flamingo vision language model [2] and incorporated regularization and adaptation techniques to tailor their applications to the nuances of radiology report generation [44]. Med-PaLM M pushed the boundaries by creating a versatile 84-billion-parameter biomedical AI system capable of addressing multiple tasks across various medical modalities [47]. In contrast to these advancements, our method, LLaVA-Rad, distinguishes itself by not only achieving superior performance across several benchmark metrics but also by being comparatively lightweight. This attribute is particularly important, as it offers a more accessible and efficient solution for scaling radiology report generation, addressing both the need for factual correctness and the practicality of deployment in clinical settings.

While LLaVA-Rad represents a significant advancement in medical foundation models, our research acknowledges several areas for future exploration and improvement. First, the current scope of LLaVA-Rad is limited to CXRs. While CXR is the most common medical image examination, future iterations should evaluate the feasibility of our method on alternative anatomies (e.g., abdomen or extremities) and modalities (e.g., computed tomography or ultrasound) to enhance the model’s applicability and utility across diverse application scenarios. Attention-based attribution methods have been found to be more effective at explaining model decisions and to be more useful by radiologists [50], and our attention visualization technique does appear to highlight sensible patterns. However, alternative saliency-based methods for CXR interpretation algorithms such as Grad-CAM have been shown to have limited correlation with expert assessments and limited robustness to input perturbations [42, 55]. There is a pressing need for a more exhaustive evaluation of such grounding strategies. These would further improve the model’s explainability and interpretability, making it

more transparent and trustworthy for clinical use. Another consideration is the inherently multimodal nature of modern medical practice, which integrates various patient information streams, including historical medical images, medical records, lab tests, and vital signs. Integrating these diverse and longitudinal data sources into medical foundation models like LLaVA-Rad could significantly enrich the model's understanding and analysis, leading to more nuanced and holistic patient assessments.

LLaVA-Rad exemplifies a significant leap toward making advanced clinical reasoning capabilities accessible with limited computational resources, thus paving the way for broader clinical applications and impact. The pursuit of open-source, lightweight, high-performing models that not only extends to various medical imaging types but also incorporates multimodality and interpretability, embodies the next frontier in medical foundation model development. Such advancements will bridge the gap between current technological capabilities and the real-world demands in clinical applications, moving us closer to achieving meaningful improvements in patient outcomes.

## Methods

### Details of the dataset

**CXR-697K** We compiled a comprehensive dataset comprising 697 thousand pairs of CXR images, each accompanied by its corresponding radiology report, for pre-training the image encoder of LLaVA-Rad. This dataset amalgamates data from seven publicly available datasets as summarized in **Supplementary Table 4**. To maintain transparency and reproducibility, we adhere to the original train/val/test splits provided by each contributing public dataset, using only the train split for pre-training the image encoder.

The CheXpert dataset [24] consists of retrospectively collected chest radiographic studies conducted between October 2002 and July 2017, encompassing both inpatient and outpatient centers at Stanford Hospital. BraX [41], obtained from chest radiography studies at Hospital Israelita Albert Einstein (HIAE) before the COVID-19 pandemic in São Paulo, Brazil, was labeled for 14 radiological findings using the CheXpert Label Extraction Algorithm [24], which was adapted to detect findings in Portuguese for this dataset. CandidPTX [14] encompasses data acquired between January 2010 and April 2020 from Dunedin Hospital in New Zealand. This dataset’s chest radiographs were manually annotated by RANZCR radiology trainees and radiologists with respect to pneumothoraces, acute rib fractures, and intercostal chest tubes. VinDR [37] was gathered from HMMH and H108 hospitals in Vietnam between 2018 and 2020, with images labeled for six diagnoses by multiple experienced radiologists from these institutions. JF Healthcare [17] data was collected from approximately 300 township hospitals in China and manually annotated by multiple radiologists to identify foreign objects within the lung field on CXRs. These datasets are comprised of images and associated binary labels that indicate whether common disease entities such as *pneumonia*, or *pneumothorax* are present in the image. However, they lack free-text reports. Thus, to enable pre-training of our image encoder using image and text methods, we create synthetic reports grounded on the labels provided. Detailed templates used for this synthetic rule-based generation can be found in **Supplementary Table 5**.

MIMIC-CXR comprises images and their corresponding radiology reports sourced from radiographic studies conducted at the Beth Israel Deaconess Medical Center in Boston, MA, spanning the years 2011 to 2016 [26]. PadChest [6] encompasses CXRs interpreted and reported by 18 radiologists at the Hospital Universitario de San Juan, Alicante (Spain), covering the period from January 2009 to December 2017, alongside their corresponding reports in Spanish. For this data, we harness the capabilities of GPT-4 to translate these reports into English, ensuring linguistic consistency.

**MIMIC-CXR** free-text reports are utilized for training the text-generation component of LLaVA-Rad. For each report, we extract the *Indication*, *Findings* and *Impression* sections. To do so, we employ rule-based heuristics as supported by the official MIMIC code repository.

Extracting reports in this rule-based manner poses two challenges. First, report structure varies within the dataset, with use of different section headers, merging of findings and impression into the same section, etc., which limits the availability of reports with findings available. Second, reports often contain references to prior examinations, such as "heart size remains unchanged". This poses a challenge for training report generation systems which often hallucinate references to prior examinations that are not available at inference time [40]. To mitigate these challenges, we leverage GPT-4 to extract the reason for exam, findings, and impression sections in the free-text reports from MIMIC-CXR. Prompt templates used to instruct GPT-4 for the organization are elaborated in **Supplementary Table 6**. Compared to the standard MIMIC-CXR rule-based extraction method, GPT-4 demonstrates proficiency in enhancing report quality by addressing issues like grammar errors, broken words, and synonymous section headers, while at the same time eliminating redundant phrases and references to previous exams. **Supplementary Table 7** showcases examples of sections structured by GPT and those extracted through rule-based methods. The use of GPT to extract sections augments rule-based data by an additional 237, 073 image-text pairs for the training split and 1, 952 for the validation split, as summarized in **Supplementary Table 3**.

### Modeling Approach

**Image Encoder** Within the LLaVA framework, the image encoder plays a pivotal role in extracting complex image representations, crucial for tasks such as automated medical report generation where standard vision transformer models often do not capture the necessary detail and nuanced



representations (**Supplementary Table 8**). To overcome this, we pretrain a domain-specific vision encoder, named BiomedCLIP-CXR, and integrate it into LLaVA to bolster its medical image analysis capabilities. Our method includes several key enhancements: firstly, we increase the image input resolution to 518px, substantially higher than the 224px or 336px resolutions typically used in LLaVA-Med, to capture more detailed image features. Secondly, we compile the CXR-697K dataset, an extensive collection of over 697 thousand CXR images from various sources, providing a rich foundation for pretraining. Lastly, we employ the BiomedCLIP recipe for training BiomedCLIP-CXR, which involves contrastive vision-language training with PubMedBERT, a text encoder specialized for the medical domain [56]. The initialization of our vision encoder uses a DINOv2 model checkpoint, benefiting from its extensive training on a diverse set of 142 million general-domain images [38].

**Small Multimodal Model** LLaVA-Rad follows LLaVA [31, 30] and LLaVA-Med [29] which leverage the capabilities of a pre-trained image encoder and a pre-trained language model to create a SMM. We choose BiomedCLIP-CXR as our image encoder and Vicuna-7B-v1.5 [9] as our language model. A multi-layer perceptron (MLP), which is randomly initialized, is introduced to project image features extracted by the image encoder into the word embedding space of the language model. Conditioned on the projected image features (visual tokens) and textual tokens, LLaVA-Rad generates text in an autoregressive manner. We refer the reader to LLaVA [31, 30] for a more in-depth description of the model architecture.

**Training Strategy** Due to the introduction of our domain-specific image encoder BiomedCLIP-CXR, LLaVA-Rad is not initialized with the pre-trained LLaVA weights. Instead, we initialize LLaVA-Rad with the pre-trained image encoder BiomedCLIP-CXR, the pre-trained language model Vicuna-7B-v1.5, and a randomly initialized MLP. Similar to LLaVA and LLaVA-Med, the SMM training procedure is done in two stages, feature alignment and end-to-end fine-tuning. Given a set of training examples, where each example consists of a CXR  $X_v$  and the corresponding indication section  $X_i$  and finding section  $X_f$  from the processed report, the training procedure is described as follows:

In the feature alignment stage, we freeze the image encoder and the language model, and only update the MLP projection layer. Given a CXR  $X_v$ , we train LLaVA-Rad to generate the corresponding findings section  $X_f$ . Note that the indication section  $X_i$  is not used in this stage. No text prompt is used, and the image is the only input. Our goal is to align the image features with word embeddings of the language model via the learning of the projection layer. In this stage, we train LLaVA-Rad on the training split of MIMIC-CXR for 1 epoch.

In the end-to-end fine-tuning stage, we train both the MLP projection layer and the language model. However, unlike the majority of existing work that fully fine-tunes the language model, we apply the parameter efficient fine-tuning method LoRA [19], which has recently been shown to achieve comparable performance to full fine-tuning while significantly reducing the training cost [13, 33]. Given a CXR  $X_v$  and the corresponding indication section  $X_i$ , we train LLaVA-Rad to generate the finding section  $X_f$ , using the training split of MIMIC-CXR. Similar to the approaches taken by LLaVA and LLaVA-Med, our training process utilizes cross-entropy loss, applied in an auto-regressive manner, to optimize the generation of reports.

## Model Evaluation

Our model evaluation consists of cross-modal retrieval evaluation, where we evaluate the quality of alignment between LLaVA-Rad’s CXR their corresponding reports, attention visualization, which illustrates the level of grounding the model’s text predictions with regions of the input image, and the automated report evaluation which studied factual correctness and lexical similarity metrics and their alignment with radiologist error quantification. To ensure a thorough evaluation, the model is tested not only on a held-out subset of the MIMIC-CXR dataset, but also on a held-out subset of the CheXpert (n=63) and Open-I [12] (n=2,163) datasets. Notably, CheXpert CXRs from the training set were used alongside synthetic label-derived reports to train the image encoder, but the held-out evaluation set, derived from the CheXpert validation split, contains CXRs and radiologist reports that were not available during training. Alternatively, the Open-I dataset was fully held out during model development. The inclusion of CheXpert and Open-I tests the external generalizability and adaptability of the model across different datasets with varying degrees of familiarity and complexity.

## Image-Text Alignment

**Cross-modal retrieval evaluation** This task consists of matching radiology reports to their corresponding radiology images (text-to-image) and the reverse (image-to-text), thus evaluating the model’s ability to identify corresponding CXRs and reports by calculating similarity scores between images and text. We compared the performance of LLaVA-Rad, which uses the specialized BiomedCLIP-CXR, with more general image encoders used for LLaVA-Med and LLaVA, namely BiomedCLIP and OpenAI CLIP models. We used the official MIMIC-CXR test set for evaluation, quantifying performance using recall at K, a commonly used retrieval evaluation metric that measures the share of relevant items captured within the top K positions.

**Attention Visualization** To qualitatively examine how well LLaVA-Rad’s image and text align, we visualize the model’s attention mechanisms during its generative process. Specifically, we focus on analyzing LLaVA-Rad’s attention to each image token while generating words. This analysis enables us to understand how well each generated word aligns with relevant regions within the image. To achieve this, we conduct an in-depth examination of a fully trained LLaVA-Rad model across all its 32 layers and 32 attention heads. Furthermore, to provide a clearer insight into the model’s attention patterns, we calculate either the mean or maximum values (or both) across all layers and heads. For visualization purposes, we reformat the attention matrices into a 37x37 grid to mirror the original spatial dimensions of the image tokens.

## Quality of Generated Reports

**Existing Evaluation Metrics** We employ a suite of automatic evaluation metrics to determine the quality of generated reports. We report commonly used lexical similarity metrics (ROUGE-L, BLEU-4) for the sake of comparison with prior methods. However, we focus our model development on factual correctness metrics, employing commonly used metrics such as F1-CheXbert and F1-RadGraph, as well as proposing an automatic GPT scoring-based metric, CheXprompt. The F1-CheXbert metric [57] corresponds to the F1 score of extracted disease labels of a generated report compared to the reference, as determined by the CheXbert labeler [43]. In line with prior work, we report F1-CheXbert for all 14 CheXbert classes, in addition to that over 5 classes that represent the most common findings in real-world CXR reports (atelectasis, cardiomegaly, consolidation, edema, and pleural effusion). The F1-RadGraph metric [11] broadens the scope of the factual correctness evaluation by comparing the agreement of anatomy and observation entities extracted from the candidate report with that of the reference. Prior to this work, the F1-RadGraph metric was considered as a reference for the evaluation of factual correctness in radiology reports. However, it has limited correlation with manual error scoring as performed by radiologists, which has led to the proposal of composite metrics such as RadCliQ that aim to better reflect human evaluation of factual correctness [52].

**CheXprompt** Given the limitations of existing report evaluation methods and the challenge of accurately evaluating generated reports at scale, we explore the utility of a language model-based scoring system, which has shown success in other domains [32, 48, 15]. Specifically, we employ GPT as an evaluator that quantifies the presence of the following six error types, as per [52]: false prediction of finding, omission of finding, incorrect location/position of finding, incorrect severity of finding, mention of comparison that is not present in the reference, omission of comparison describing a change from a previous study. We instruct GPT to quantify the number of errors of each of the six error types, keeping a separate count for clinically insignificant and significant errors. In each rating prompt, we include a fixed set of five example report evaluation pairs alongside mean error counts for each type to enable the model to leverage in-context examples that quantify errors as requested. We evaluate the validity of the proposed CheXprompt using the ReXval dataset [53], which is comprised of error annotations from 6 board certified radiologists on 200 pairs of candidate and ground-truth reports, where each radiologist provides counts of each of the 6 aforementioned error types, also discriminating between clinically significant and insignificant errors.

For comparison, we evaluate the performance of three types of GPT models: GPT-3.5 Turbo (GPT-3.5T), GPT-4, and GPT-4-Turbo (GPT-4T). We quantify the alignment between errors quantified by radiologists with that of existing report evaluation methods, in addition to CheXprompt, using Kendall’s Tau b coefficient (rank correlation coefficient). Further, we directly compare the performance of CheXprompt based on GPT-4T with that of each radiologist in a leave-one-rater-out fashion. For each comparison with a rater, the mean of the remaining left-in radiologist raters was

calculated. The paired interobserver difference between the held-out radiologist rater and the mean was compared to the paired interobserver difference between CheXprompt and the mean. The mean absolute interobserver difference (MAD) for each left-out radiologist was compared with that of CheXprompt, with statistical significance determined using paired t-tests.

Finally, we use the GPT-4T version of CheXprompt to quantify the total number of clinically significant and overall errors in each generated report in the evaluation datasets. We quantify these totals in reports from publicly accessible models, enabling us to compare LLaVA-Rad with LLaVA-Med, LLaVA, CheXagent, and GPT-4V. Further, we study the overall proportion of error-free reports in the evaluation datasets, reflecting the potential of each model in directly impacting radiology workflows.

### **Data availability**

We will provide scripts to reproduce CXR-697K and MIMIC-CXR from the original datasets, upon publication of this manuscript.

### **Code availability**

LLaVA-Rad will be made fully available upon publication, including the model weights and relevant source code for pre-training, fine-tuning, and inference. We will also provide detailed methods and implementation steps to facilitate independent replication. The code to reproduce CheXprompt is publicly available at <https://aka.ms/chexprompt>.

## References

- [1] Nurbanu Aksoy, Nishant Ravikumar, and Alejandro F Frangi. Radiology report generation using transformers conditioned with non-imaging data. In *Medical Imaging 2023: Imaging Informatics for Healthcare, Research, and Applications*, volume 12469, pages 146–154. SPIE, 2023.
- [2] Jean-Baptiste Alayrac, Jeff Donahue, Pauline Luc, Antoine Miech, Iain Barr, Yana Hasson, Karel Lenc, Arthur Mensch, Katherine Millican, Malcolm Reynolds, et al. Flamingo: a visual language model for few-shot learning. *Advances in Neural Information Processing Systems*, 35:23716–23736, 2022.
- [3] Shekoofeh Azizi, Laura Culp, Jan Freyberg, Basil Mustafa, Sebastien Baur, Simon Kornblith, Ting Chen, Patricia MacWilliams, S Sara Mahdavi, Ellery Wulczyn, et al. Robust and efficient medical imaging with self-supervision. *arXiv preprint arXiv:2205.09723*, 2022.
- [4] Shekoofeh Azizi, Basil Mustafa, Fiona Ryan, Zachary Beaver, Jan Freyberg, Jonathan Deaton, Aaron Loh, Alan Karthikesalingam, Simon Kornblith, Ting Chen, Vivek Natarajan, and Mohammad Norouzi. Big self-supervised models advance medical image classification. *arXiv preprint arXiv:2101.05224*, 2021.
- [5] Rishi Bommasani, Drew A Hudson, Ehsan Adeli, Russ Altman, Simran Arora, Sydney von Arx, Michael S Bernstein, Jeannette Bohg, Antoine Bosselut, Emma Brunskill, et al. On the opportunities and risks of foundation models. *arXiv preprint arXiv:2108.07258*, 2021.
- [6] Aurelia Bustos, Antonio Pertusa, Jose-Maria Salinas, and Maria De La Iglesia-Vaya. Padchest: A large chest x-ray image dataset with multi-label annotated reports. *Medical image analysis*, 66:101797, 2020.
- [7] Zhihong Chen, Yan Song, Tsung-Hui Chang, and Xiang Wan. Generating radiology reports via memory-driven transformer. *arXiv preprint arXiv:2010.16056*, 2020.
- [8] Zhihong Chen, Maya Varma, Jean-Benoit Delbrouck, Magdalini Paschali, Louis Blankemeier, Dave Van Veen, Jeya Maria Jose Valanarasu, Alaa Youssef, Joseph Paul Cohen, Eduardo Pontes Reis, et al. Chexagent: Towards a foundation model for chest x-ray interpretation. *arXiv preprint arXiv:2401.12208*, 2024.
- [9] Wei-Lin Chiang, Zhuohan Li, Zi Lin, Ying Sheng, Zhanghao Wu, Hao Zhang, Lianmin Zheng, Siyuan Zhuang, Yonghao Zhuang, Joseph E. Gonzalez, Ion Stoica, and Eric P. Xing. Vicuna: An open-source chatbot impressing gpt-4 with 90%\* chatgpt quality, March 2023.
- [10] Jan Clusmann, Fiona R Kolbinger, Hannah Sophie Muti, Zunamys I Carrero, Jan-Niklas Eckardt, Narmin Ghaffari Laleh, Chiara Maria Lavinia Löffler, Sophie-Caroline Schwarzkopf, Michaela Unger, Gregory P Veldhuizen, et al. The future landscape of large language models in medicine. *Communications Medicine*, 3(1):141, 2023.
- [11] Jean-Benoit Delbrouck, Pierre Chambon, Christian Bluethgen, Emily Tsai, Omar Almusa, and Curtis Langlotz. Improving the factual correctness of radiology report generation with semantic rewards. In *Findings of the Association for Computational Linguistics: EMNLP 2022*, pages 4348–4360, Abu Dhabi, United Arab Emirates, December 2022. Association for Computational Linguistics.
- [12] Dina Demner-Fushman, Sameer Antani, Matthew Simpson, and George R Thoma. Design and development of a multimodal biomedical information retrieval system. *Journal of Computing Science and Engineering*, 6(2):168–177, 2012.
- [13] Tim Dettmers, Artidoro Pagnoni, Ari Holtzman, and Luke Zettlemoyer. Qlora: Efficient finetuning of quantized llms, 2023.
- [14] Sijing Feng, Damian Azzollini, Ji Soo Kim, Cheng Kai Jin, Eve Kim, Simon Gordon, Jason Yeoh, Min A Han, Andrew Lee, Aakash Patel, Martin Urschler, Amy Fong, Cameron Simmers, Gregory Tarr, Stuart Barnard, and Ben Wilson. CANDID-PTX. *Radiology: Artificial Intelligence*, 6 2021.
- [15] Fabrizio Gilardi, Meysam Alizadeh, and Maël Kubli. Chatgpt outperforms crowd-workers for text-annotation tasks. *arXiv preprint arXiv:2303.15056*, 2023.
- [16] Suriya Gunasekar, Yi Zhang, Jyoti Aneja, Caio César Teodoro Mendes, Allie Del Giorno, Sivakanth Gopi, Mojan Javaheripi, Piero Kauffmann, Gustavo de Rosa, Olli Saarikivi, Adil

- Salim, Shital Shah, Harkirat Singh Behl, Xin Wang, Sébastien Bubeck, Ronen Eldan, Adam Tauman Kalai, Yin Tat Lee, and Yuanzhi Li. Textbooks are all you need, 2023.
- [17] JF Healthcare. Object-cxr - automatic detection of foreign objects on chest x-rays. <https://web.archive.org/web/20201127235812/https://jfhealthcare.github.io/object-CXR/>.
- [18] Xiaodi Hou, Zhi Liu, Xiaobo Li, Xingwang Li, Shengtian Sang, and Yijia Zhang. Mkl: Medical knowledge with contrastive learning model for radiology report generation. *Journal of Biomedical Informatics*, 146:104496, 2023.
- [19] Edward J Hu, yelong shen, Phillip Wallis, Zeyuan Allen-Zhu, Yuanzhi Li, Shean Wang, Lu Wang, and Weizhu Chen. LoRA: Low-rank adaptation of large language models. In *International Conference on Learning Representations*, 2022.
- [20] Jonathan Huang, Luke Neill, Matthew Wittbrodt, David Melnick, Matthew Klug, Michael Thompson, John Bailitz, Timothy Loftus, Sanjeev Malik, Amit Phull, et al. Generative artificial intelligence for chest radiograph interpretation in the emergency department. *JAMA network open*, 6(10):e2336100–e2336100, 2023.
- [21] Shih-Cheng Huang, Akshay S Chaudhari, Curtis P Langlotz, Nigam Shah, Serena Yeung, and Matthew P Lungren. Developing medical imaging ai for emerging infectious diseases. *nature communications*, 13(1):7060, 2022.
- [22] Shih-Cheng Huang, Anuj Pareek, Malte Jensen, Matthew P Lungren, Serena Yeung, and Akshay S Chaudhari. Self-supervised learning for medical image classification: a systematic review and implementation guidelines. *NPJ Digital Medicine*, 6(1):74, 2023.
- [23] Stephanie L Hyland, Shruthi Bannur, Kenza Bouzid, Daniel C Castro, Mercy Ranjit, Anton Schwaighofer, Fernando Pérez-García, Valentina Salvatelli, Shaury Srivastav, Anja Thieme, et al. Maira-1: A specialised large multimodal model for radiology report generation. *arXiv preprint arXiv:2311.13668*, 2023.
- [24] Jeremy Irvin, Pranav Rajpurkar, Michael Ko, Yifan Yu, Silviana Ciurea-Ilcus, Chris Chute, Henrik Marklund, Behzad Haghgoo, Robyn Ball, Katie Shpanskaya, et al. Chexpert: A large chest radiograph dataset with uncertainty labels and expert comparison. In *Proceedings of the AAAI conference on artificial intelligence*, volume 33, pages 590–597, 2019.
- [25] Saahil Jain, Ashwin Agrawal, Adriel Saporta, Steven QH Truong, Du Nguyen Duong, Tan Bui, Pierre Chambon, Yuhao Zhang, Matthew P. Lungren, Andrew Y. Ng, Curtis P. Langlotz, and Pranav Rajpurkar. Radgraph: Extracting clinical entities and relations from radiology reports, 2021.
- [26] Alistair EW Johnson, Tom J Pollard, Seth J Berkowitz, Nathaniel R Greenbaum, Matthew P Lungren, Chih-ying Deng, Roger G Mark, and Steven Horng. MIMIC-CXR, a de-identified publicly available database of chest radiographs with free-text reports. *Scientific data*, 6(1):317, 2019.
- [27] Curtis P Langlotz. The future of ai and informatics in radiology: 10 predictions. *Radiology*, 309(1):e231114, 2023.
- [28] Eric Lehman, Evan Hernandez, Diwakar Mahajan, Jonas Wulff, Micah J Smith, Zachary Ziegler, Daniel Nadler, Peter Szolovits, Alistair Johnson, and Emily Alsentzer. Do we still need clinical language models? In Bobak J. Mortazavi, Tasmie Sarker, Andrew Beam, and Joyce C. Ho, editors, *Proceedings of the Conference on Health, Inference, and Learning*, volume 209 of *Proceedings of Machine Learning Research*, pages 578–597. PMLR, 22 Jun–24 Jun 2023.
- [29] Chunyuan Li, Cliff Wong, Sheng Zhang, Naoto Usuyama, Haotian Liu, Jianwei Yang, Tristan Naumann, Hoifung Poon, and Jianfeng Gao. LLaVA-med: Training a large language-and-vision assistant for biomedicine in one day. In *Thirty-seventh Conference on Neural Information Processing Systems Datasets and Benchmarks Track*, 2023.
- [30] Haotian Liu, Chunyuan Li, Yuheng Li, and Yong Jae Lee. Improved baselines with visual instruction tuning, 2023.
- [31] Haotian Liu, Chunyuan Li, Qingyang Wu, and Yong Jae Lee. Visual instruction tuning. In *Thirty-seventh Conference on Neural Information Processing Systems*, 2023.

- [32] Yang Liu, Dan Iter, Yichong Xu, Shuohang Wang, Ruochen Xu, and Chenguang Zhu. Gpteval: Nlg evaluation using gpt-4 with better human alignment. *arXiv preprint arXiv:2303.16634*, 2023.
- [33] Yadong Lu, Chunyuan Li, Haotian Liu, Jianwei Yang, Jianfeng Gao, and Yelong Shen. An empirical study of scaling instruct-tuned large multimodal models, 2023.
- [34] Arindam Mitra, Luciano Del Corro, Shweti Mahajan, Andres Cudas, Clarisse Simoes, Sahaj Agarwal, Xuxi Chen, Anastasia Razdaibiedina, Erik Jones, Kriti Aggarwal, Hamid Palangi, Guoqing Zheng, Corby Rosset, Hamed Khanpour, and Ahmed Awadallah. Orca 2: Teaching small language models how to reason, 2023.
- [35] Mashood Mohammad Mohsan, Muhammad Usman Akram, Ghulam Rasool, Norah Saleh Alghamdi, Muhammad Abdullah Aamer Baqai, and Muhammad Abbas. Vision transformer and language model based radiology report generation. *IEEE Access*, 11:1814–1824, 2022.
- [36] Michael Moor, Oishi Banerjee, Zahra Shakeri Hossein Abad, Harlan M Krumholz, Jure Leskovec, Eric J Topol, and Pranav Rajpurkar. Foundation models for generalist medical artificial intelligence. *Nature*, 616(7956):259–265, 2023.
- [37] H Nguyen, HH Pham, NT Nguyen, DB Nguyen, M Dao, V Vu, K Lam, and LT Le. Vinbigdata chest x-ray abnormalities detection. *Kaggle Competition <https://www.kaggle.com/c/vinbigdatachest-xray-abnormalities-detection>*, 2020.
- [38] Maxime Oquab, Timothée Darcet, Théo Moutakanni, Huy Vo, Marc Szafraniec, Vasil Khalidov, Pierre Fernandez, Daniel Haziza, Francisco Massa, Alaaeldin El-Nouby, Mahmoud Assran, Nicolas Ballas, Wojciech Galuba, Russell Howes, Po-Yao Huang, Shang-Wen Li, Ishan Misra, Michael Rabbat, Vasu Sharma, Gabriel Synnaeve, Hu Xu, Hervé Jegou, Julien Mairal, Patrick Labatut, Armand Joulin, and Piotr Bojanowski. Dinov2: Learning robust visual features without supervision, 2024.
- [39] Renjie Pan, Ruisheng Ran, Wei Hu, Wenfeng Zhang, Qibing Qin, and Shaoguo Cui. S3-net: A self-supervised dual-stream network for radiology report generation. *IEEE Journal of Biomedical and Health Informatics*, 2023.
- [40] Vignav Ramesh, Nathan A Chi, and Pranav Rajpurkar. Improving radiology report generation systems by removing hallucinated references to non-existent priors. In *Machine Learning for Health*, pages 456–473. PMLR, 2022.
- [41] Eduardo P Reis, Joselisa PQ de Paiva, Maria CB da Silva, Guilherme AS Ribeiro, Victor F Paiva, Lucas Bulgarelli, Henrique MH Lee, Paulo V Santos, Vanessa M Brito, Lucas TW Amaral, et al. Brax, brazilian labeled chest x-ray dataset. *Scientific Data*, 9(1):487, 2022.
- [42] Adriel Saporta, Xiaotong Gui, Ashwin Agrawal, Anuj Pareek, Steven QH Truong, Chanh DT Nguyen, Van-Doan Ngo, Jayne Seekins, Francis G Blankenberg, Andrew Y Ng, et al. Benchmarking saliency methods for chest x-ray interpretation. *Nature Machine Intelligence*, 4(10):867–878, 2022.
- [43] Akshay Smit, Saahil Jain, Pranav Rajpurkar, Anuj Pareek, Andrew Y. Ng, and Matthew P. Lungren. Chexbert: Combining automatic labelers and expert annotations for accurate radiology report labeling using bert, 2020.
- [44] Ryutaro Tanno, David GT Barrett, Andrew SELLERGEN, Sumedh Ghaisas, Sumanth Dathathri, Abigail See, Johannes Welbl, Karan Singhal, Shekoofeh Azizi, Tao Tu, et al. Consensus, dissensus and synergy between clinicians and specialist foundation models in radiology report generation. *arXiv preprint arXiv:2311.18260*, 2023.
- [45] Arun James Thirunavukarasu, Darren Shu Jeng Ting, Kabilan Elangovan, Laura Gutierrez, Ting Fang Tan, and Daniel Shu Wei Ting. Large language models in medicine. *Nature medicine*, 29(8):1930–1940, 2023.
- [46] Daniel Truhn, Gustav Müller-Franzes, and Jakob Nikolas Kather. The ecological footprint of medical ai. *European Radiology*, pages 1–3, 2023.
- [47] Tao Tu, Shekoofeh Azizi, Danny Driess, Mike Schaeckermann, Mohamed Amin, Pi-Chuan Chang, Andrew Carroll, Charles Lau, Ryutaro Tanno, Ira Ktena, Anil Palepu, Basil Mustafa, Aakanksha Chowdhery, Yun Liu, Simon Kornblith, David Fleet, Philip Mansfield, Sushant Prakash, Renee Wong, Sunny Virmani, Christopher Semturs, S. Sara Mahdavi, Bradley Green, Ewa Dominowska, Blaise Aguera y Arcas, Joelle Barral, Dale Webster, Greg S. Corrado, Yossi

- Matias, Karan Singhal, Pete Florence, Alan Karthikesalingam, and Vivek Natarajan. Towards generalist biomedical ai. *NEJM AI*, 1(3):AIoa2300138, 2024.
- [48] Jiaan Wang, Yunlong Liang, Fandong Meng, Haoxiang Shi, Zhixu Li, Jinan Xu, Jianfeng Qu, and Jie Zhou. Is chatgpt a good nlg evaluator? a preliminary study. *arXiv preprint arXiv:2303.04048*, 2023.
- [49] Jun Wang, Abhir Bhalerao, and Yulan He. Cross-modal prototype driven network for radiology report generation. In *European Conference on Computer Vision*, pages 563–579. Springer, 2022.
- [50] Alessandro Wollek, Robert Graf, Saša Čečátka, Nicola Fink, Theresa Willem, Bastian O. Sabel, and Tobias Lasser. Attention-based saliency maps improve interpretability of pneumothorax classification. *Radiology: Artificial Intelligence*, 5(2):e220187, 2023.
- [51] Michael Wornow, Yizhe Xu, Rahul Thapa, Birju Patel, Ethan Steinberg, Scott Fleming, Michael A Pfeffer, Jason Fries, and Nigam H Shah. The shaky foundations of large language models and foundation models for electronic health records. *npj Digital Medicine*, 6(1):135, 2023.
- [52] Feiyang Yu, Mark Endo, Rayan Krishnan, Ian Pan, Andy Tsai, Eduardo Pontes Reis, Eduardo Kaiser Ururahy Nunes Fonseca, Henrique Min Ho Lee, Zahra Shakeri Hossein Abad, Andrew Y Ng, et al. Evaluating progress in automatic chest x-ray radiology report generation. *Patterns*, 4(9), 2023.
- [53] Feiyang Yu, Mark Endo, Rayan Krishnan, Ian Pan, Andy Tsai, Eduardo Pontes Reis, EKV Fonseca, Henrique Lee, Zahra Shakeri, Andrew Ng, et al. Radiology report expert evaluation (rexval) dataset, 2023.
- [54] Juan M Zambrano Chaves, Nandita Bhaskhar, Maayane Attias, Jean-Benoit Delbrouck, Daniel Rubin, Andreas Loening, Curtis Langlotz, and Akshay Chaudhari. Rales: a benchmark for radiology language evaluations. In A. Oh, T. Neumann, A. Globerson, K. Saenko, M. Hardt, and S. Levine, editors, *Advances in Neural Information Processing Systems*, volume 36, pages 74429–74454. Curran Associates, Inc., 2023.
- [55] Jiajin Zhang, Hanqing Chao, Giridhar Dasegowda, Ge Wang, Mannudeep K. Kalra, and Pingkun Yan. Revisiting the trustworthiness of saliency methods in radiology ai. *Radiology: Artificial Intelligence*, 6(1):e220221, 2024. PMID: 38166328.
- [56] Sheng Zhang, Yanbo Xu, Naoto Usuyama, Hanwen Xu, Jaspreet Bagga, Robert Tinn, Sam Preston, Rajesh Rao, Mu Wei, Naveen Valluri, Cliff Wong, Andrea Tupini, Yu Wang, Matt Mazzola, Swadheen Shukla, Lars Liden, Jianfeng Gao, Matthew P. Lungren, Tristan Naumann, Sheng Wang, and Hoifung Poon. Biomedclip: a multimodal biomedical foundation model pretrained from fifteen million scientific image-text pairs, 2024.
- [57] Yuhao Zhang, Derek Merck, Emily Tsai, Christopher D Manning, and Curtis Langlotz. Optimizing the factual correctness of a summary: A study of summarizing radiology reports. In *Proceedings of the 58th Annual Meeting of the Association for Computational Linguistics*, pages 5108–5120, 2020.

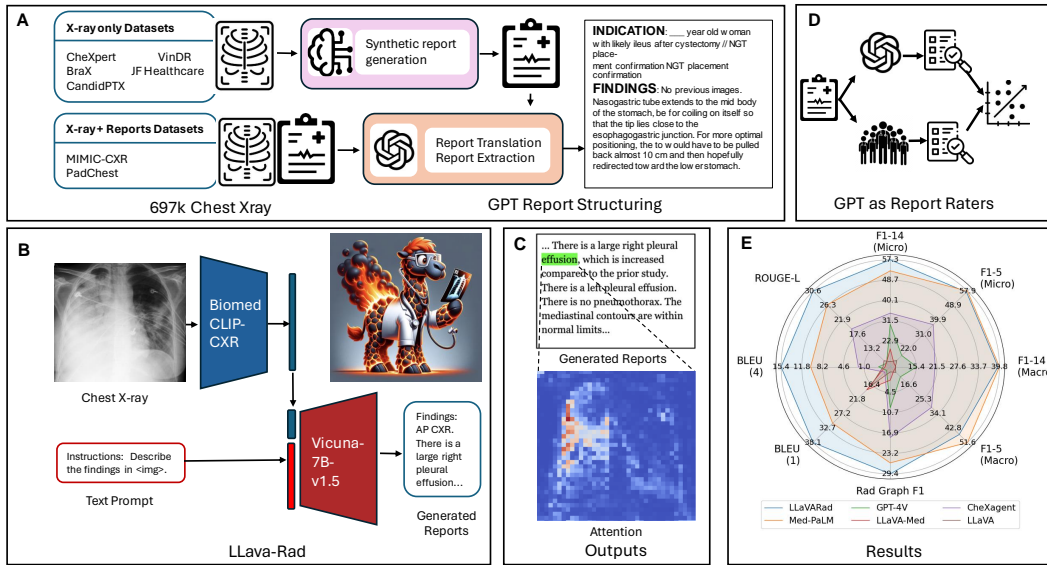


Figure 1: **LLaVA-Rad Overview**. **A**, To train LLaVA-Rad, we assemble a large dataset with over 697 thousand chest X-ray image-text pairs; GPT-4 is used to process and structure the corresponding radiology reports. **B**, We adopt a modular approach by incorporating state-of-the-art pre-trained models for individual modalities and focusing on training lightweight adapters. **C**, A qualitative visualization of the model’s attention during its generative process. **D**, For evaluation, we also propose a novel factual error scoring approach using GPT-4 and demonstrate its parity with expert evaluation. **E**, LLaVA-Rad outperforms much larger models like GPT-4V and Med-PaLM M on prior standard metrics



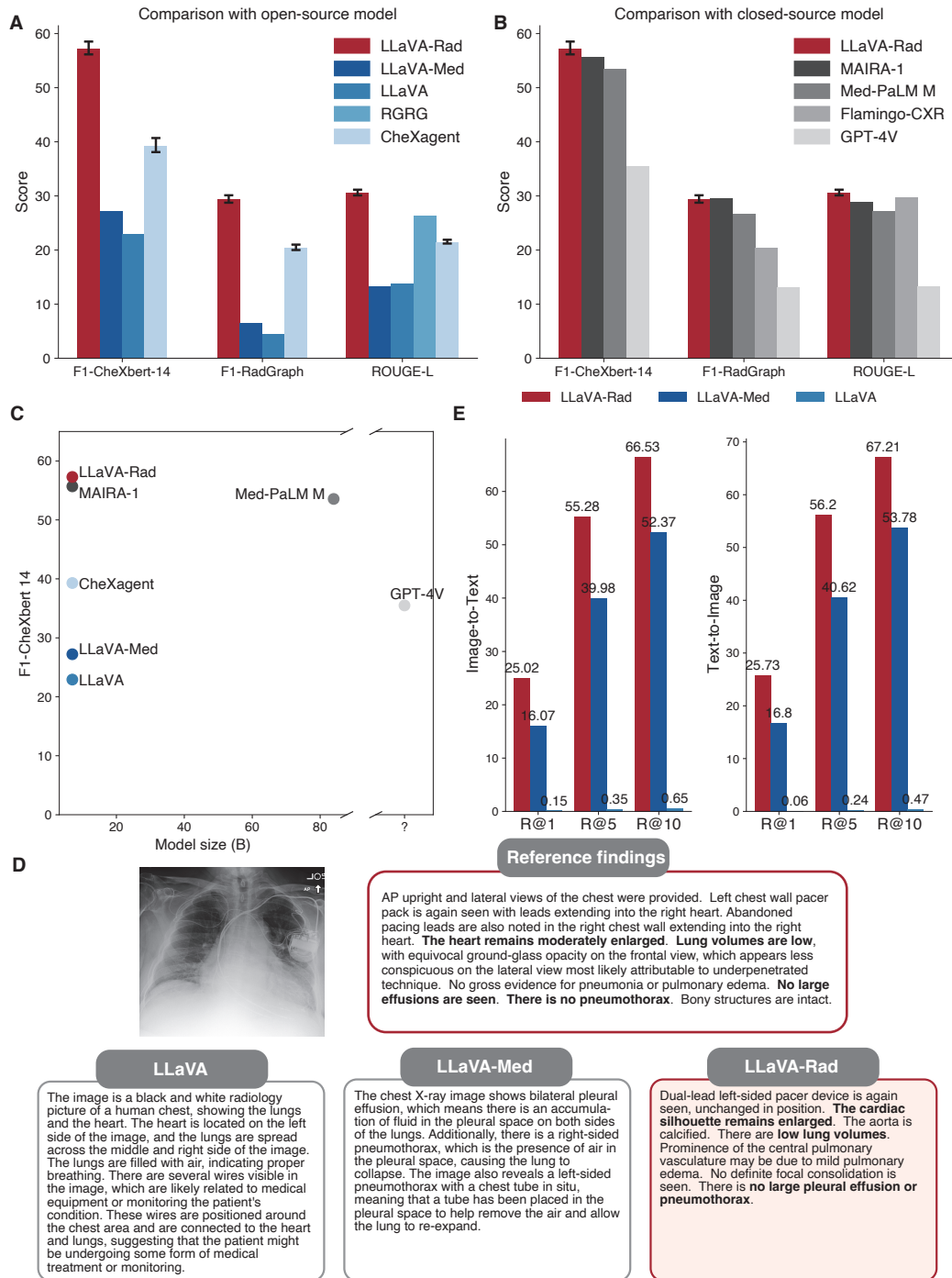


Figure 2: **Quantitative and qualitative evaluation of LLaVA-Rad using existing report generation benchmarks.** **A**, Comparison between LLaVA-Rad and open-source models according to existing preferred factual correctness and lexical similarity metrics. **B**, Comparison between LLaVA-Rad and closed-source models according to existing preferred factual correctness and lexical similarity metrics. **C**, Comparison between model size and factual correctness shows that LLaVA-Rad is both smaller and more factually correct compared to existing approaches. **D**, Illustration of a sample generated report from LLaVA-Rad compared with that of LLaVA and LLaVA-Med. LLaVA-Rad's generations that match reference findings are highlighted. **E**, Comparison of the performance on cross-modal retrieval demonstrated by LLaVA-Rad, LLaVA-Med and LLaVA.

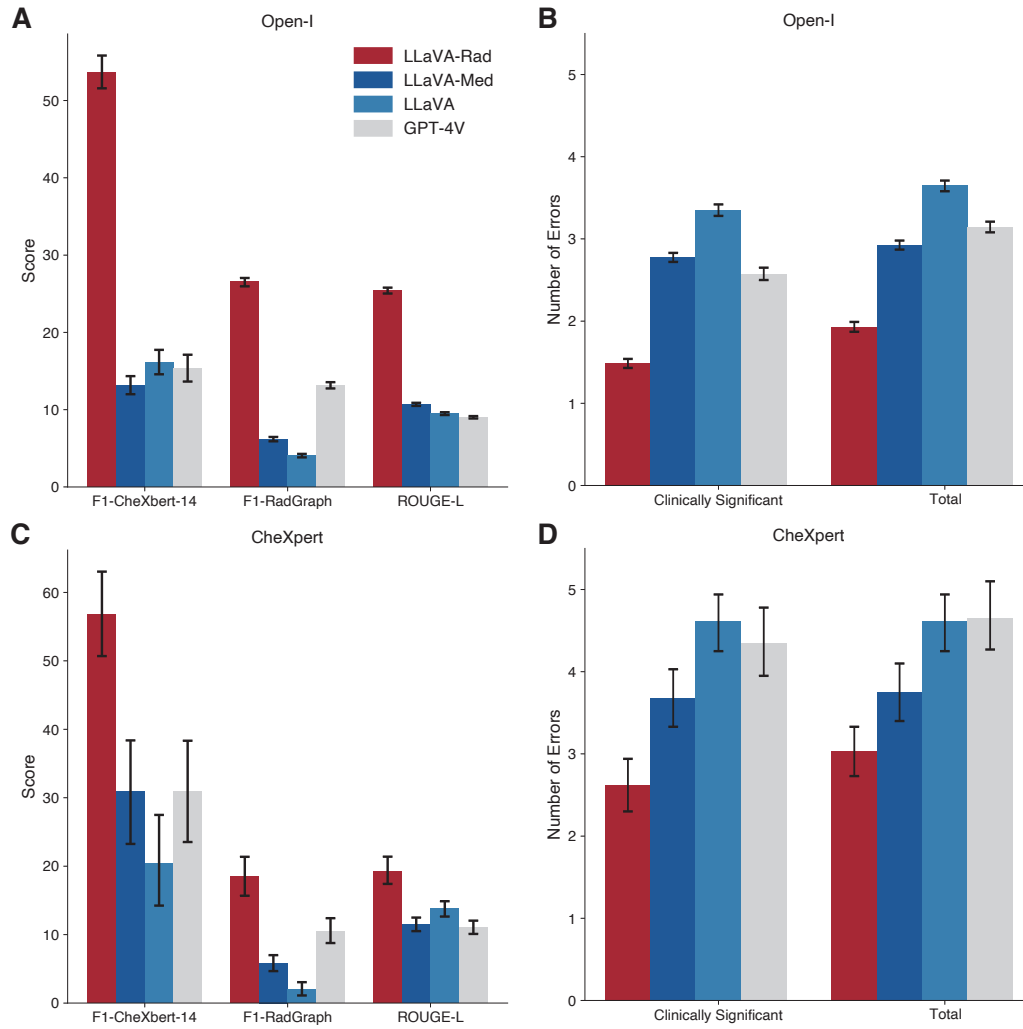


Figure 3: External validation results for LLaVA-Rad on held out Open-I (n=2,163, panels **A** and **B**) and CheXpert (n=63, panels **C** and **D**) datasets.

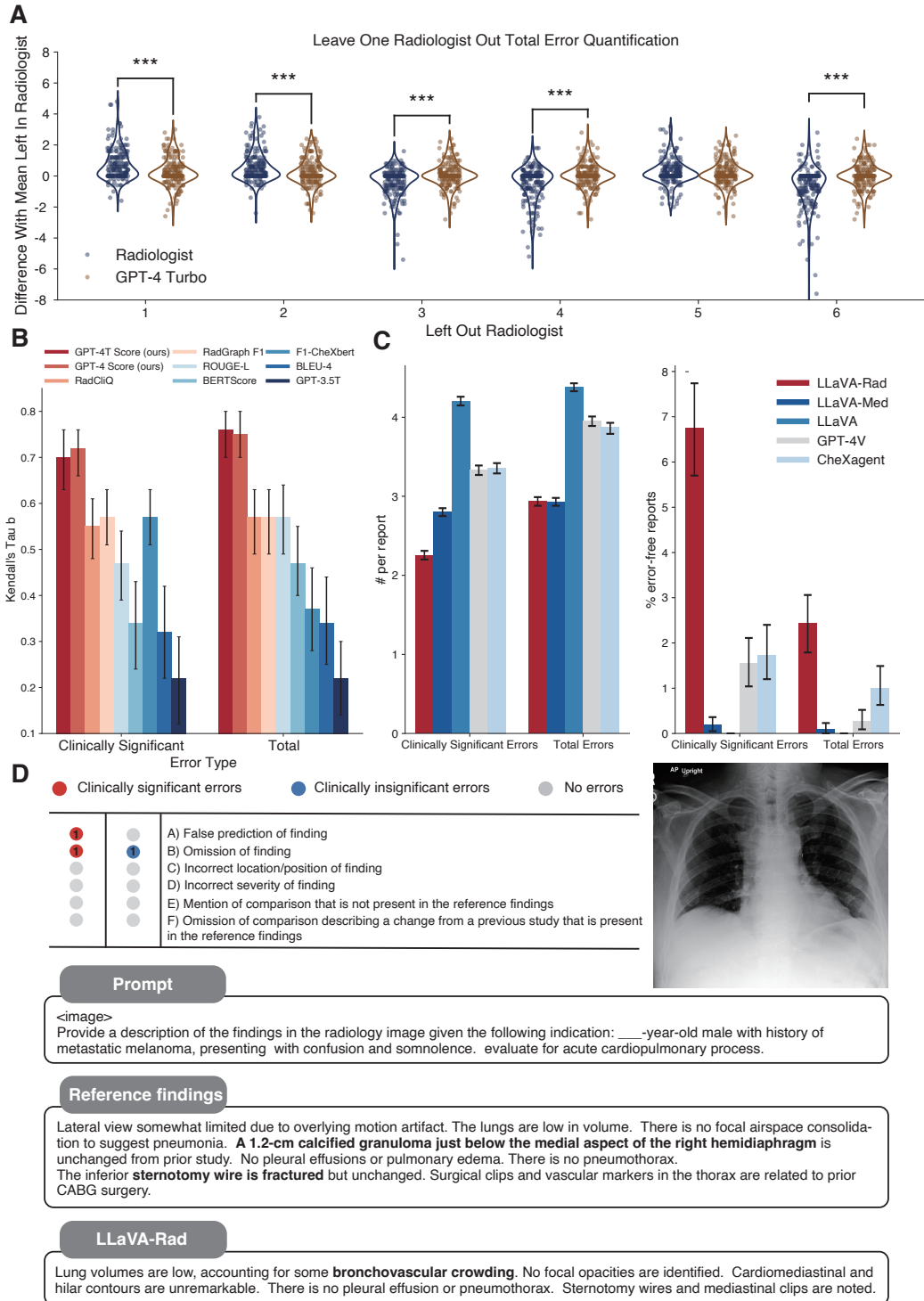


Figure 4: **Evaluating LLaVA-Rad using CheXprompt.** GPT-4T stands for GPT-4 Turbo. **A**, GPT-4 based CheXprompt is more similar to average left-in radiologists in total error quantification, compared to the left-out radiologist (mean absolute difference 0.55 vs 0.71). **B**, Comparison between CheXprompt and existing metrics in terms of agreement with radiologist error quantification. **C**, Comparison between LLaVA-Rad and competing methods using CheXprompt on the MIMIC-CXR test set. **D**, Illustration of how CheXprompt can be used to evaluate a report generated by LLaVA-Rad, with errors highlighted.

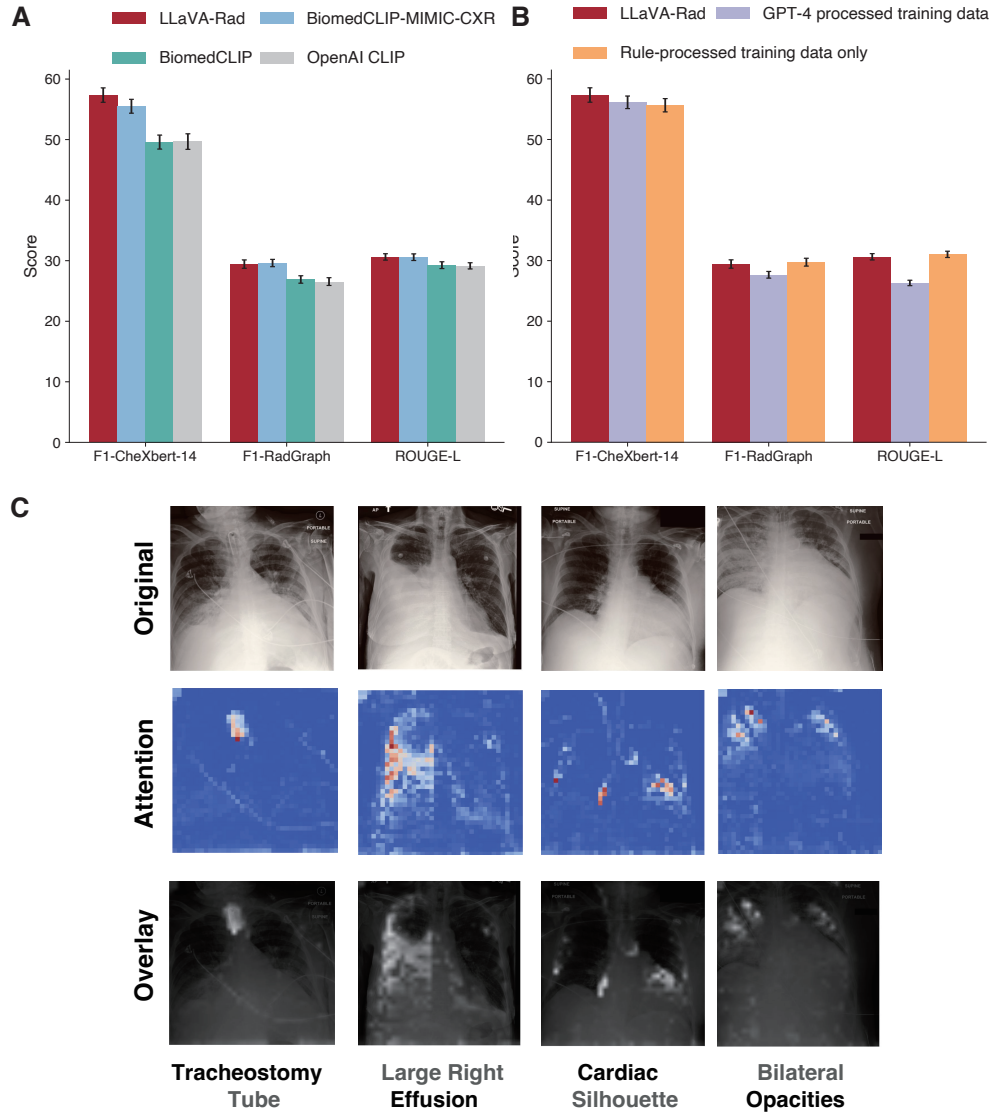
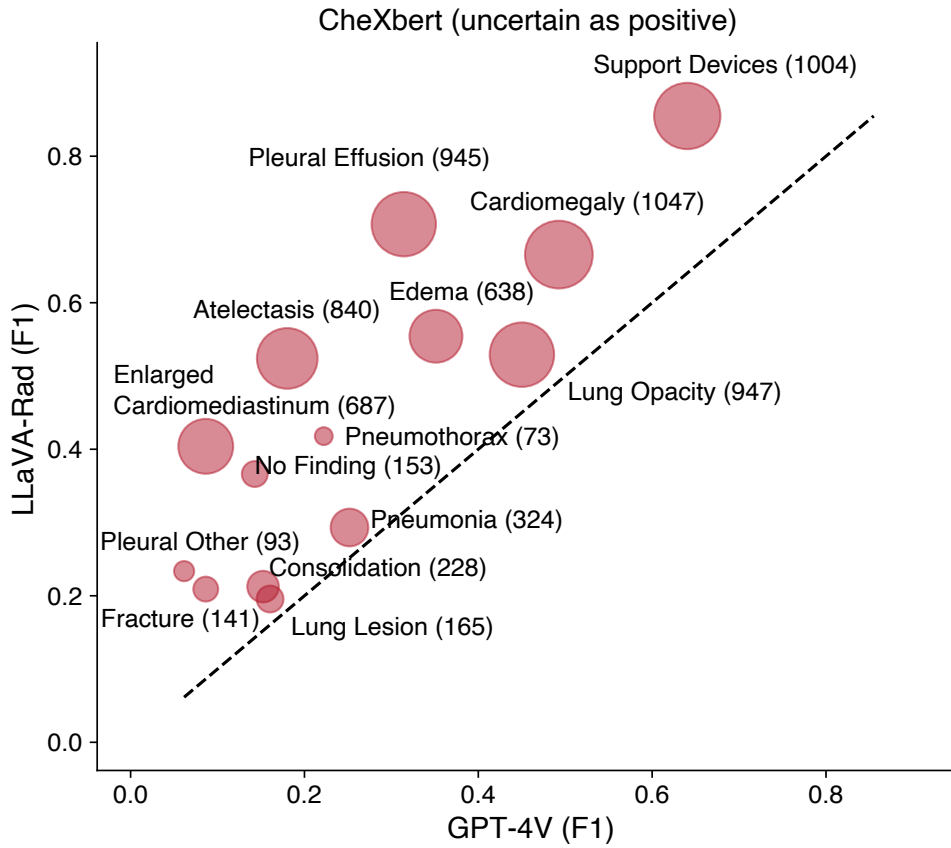
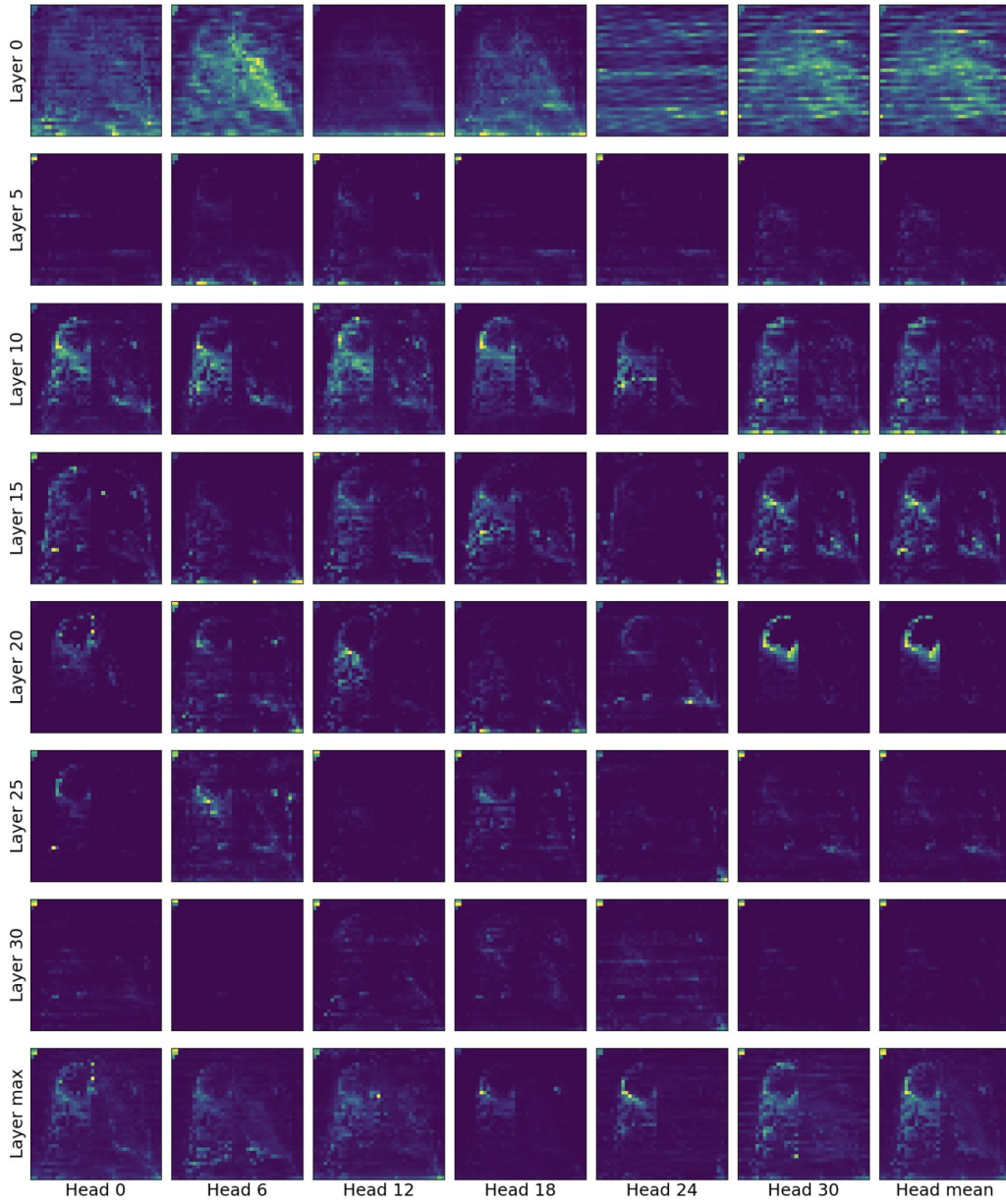


Figure 5: **Analyzing the performance of LLaVA-Rad using ablation studies and attention visualization.** **A**, Comparison of using different image encoders (from LLaVA-Rad (BiomedCLIP-CXR), BiomedCLIP continually pre-trained on MIMIC-CXR, BiomedCLIP, and OpenAI CLIP) to start the alignment and fine-tuning stages. **B**, Ablation study on only using rule-processed MIMIC-CXR training data or GPT-4 processed training data in alignment and fine-tuning stages. **C**, Attention visualization qualitatively demonstrates the appropriate grounding of LLaVA-Rad in specific image regions when generating a word (**bold**) as part of a specific finding (bottom row).

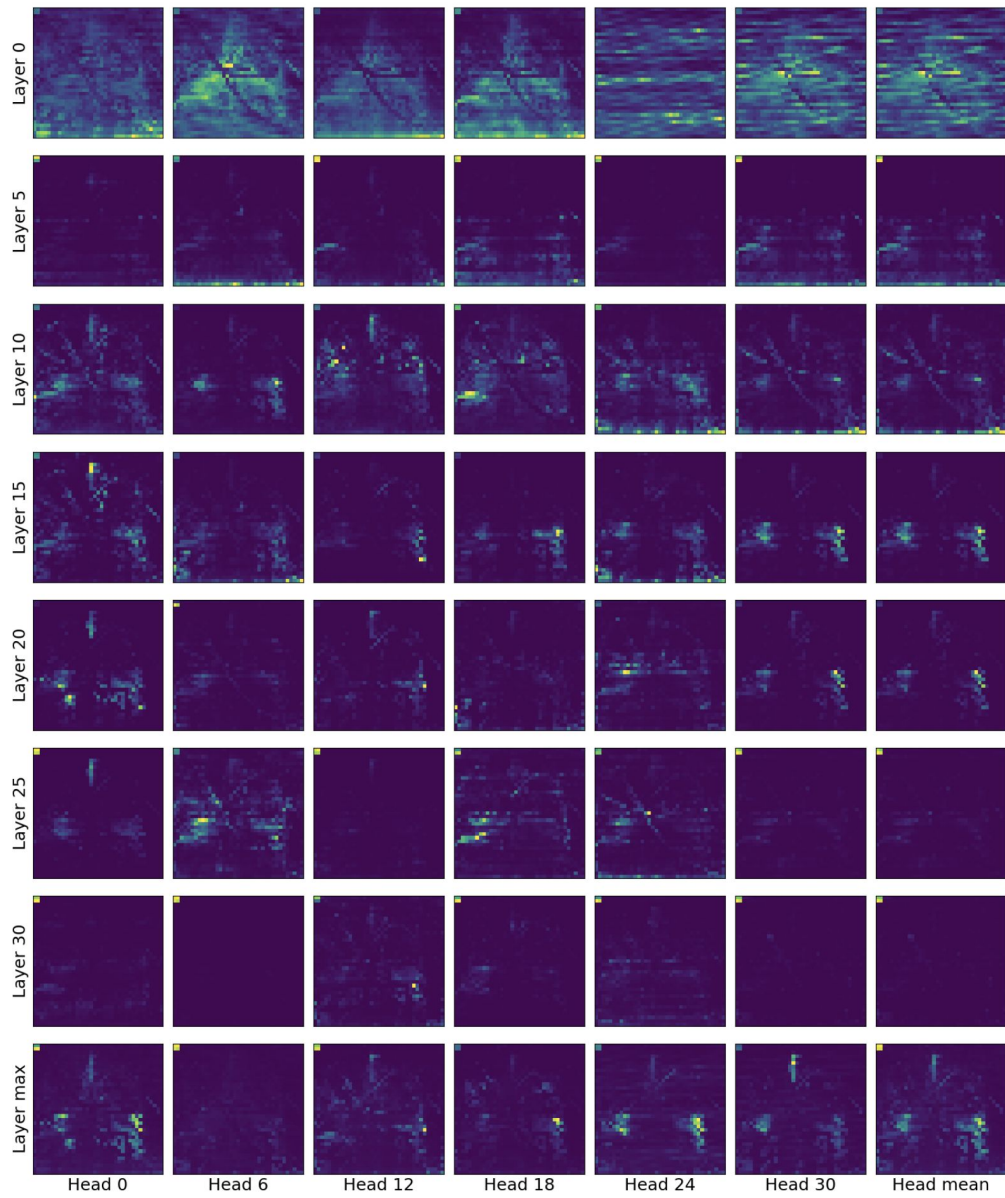
## Supplementary Information



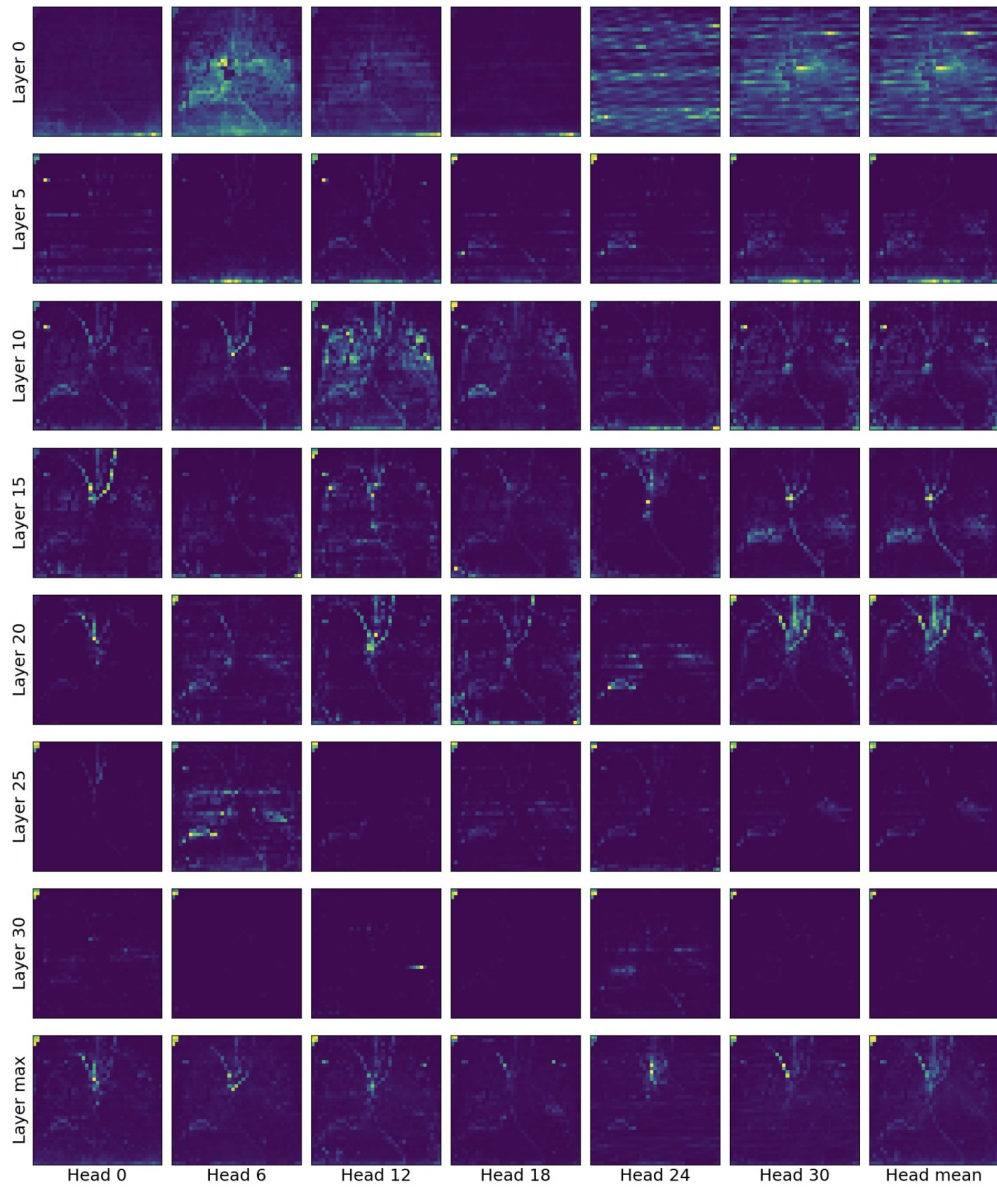
Supplementary Figure 1: Breakdown comparison between LLaVA-Rad and GPT-4V on 14 observations extracted by CheXbert from generated reports for the MIMIC-CXR test set. The circle size is proportional to the number of occurrences of each observation in the reference reports, also provided in parentheses following each observation label.



Supplementary Figure 2: Attention weights for the generated word **Effusion** from different layers and heads of the model.

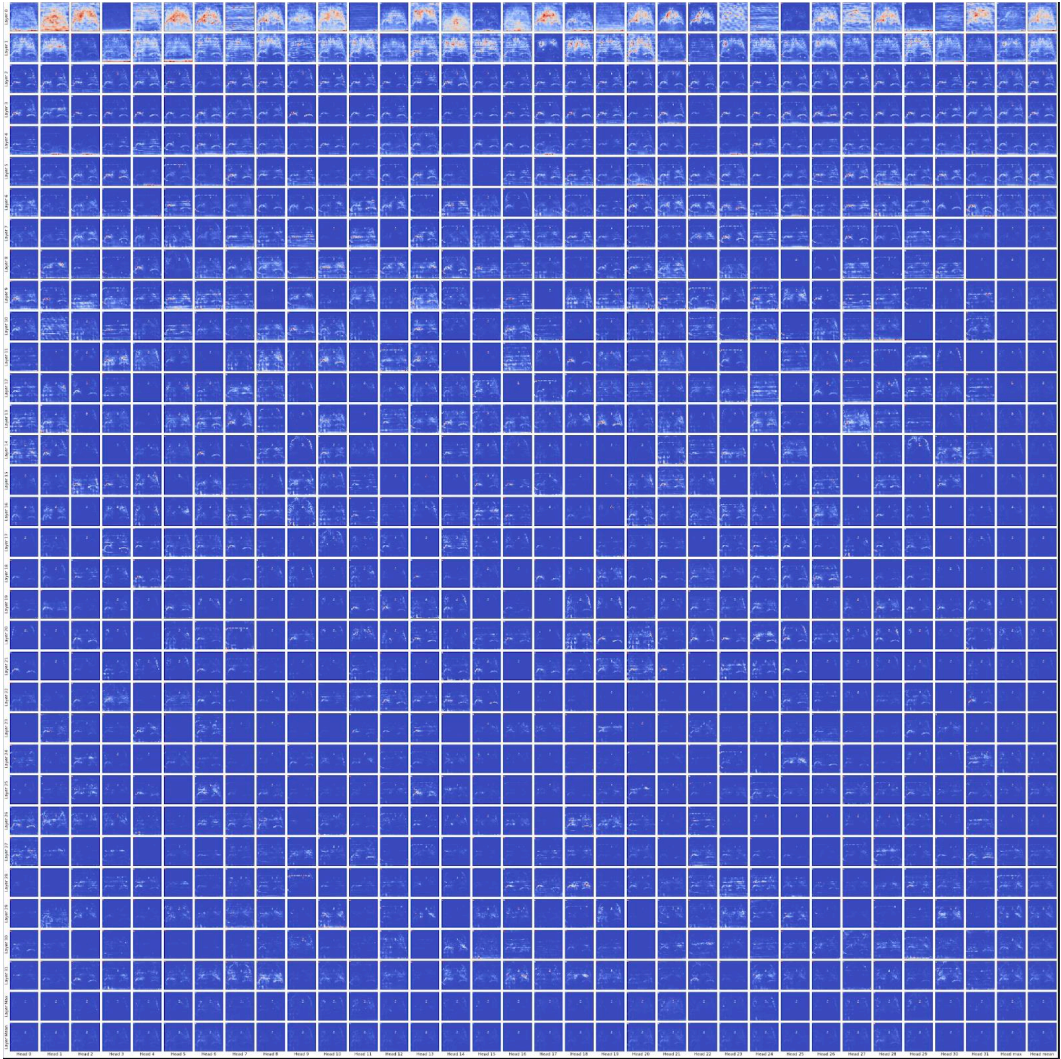


Supplementary Figure 3: Attention weights for the generated word **Opacification** from different layers and heads of the model.

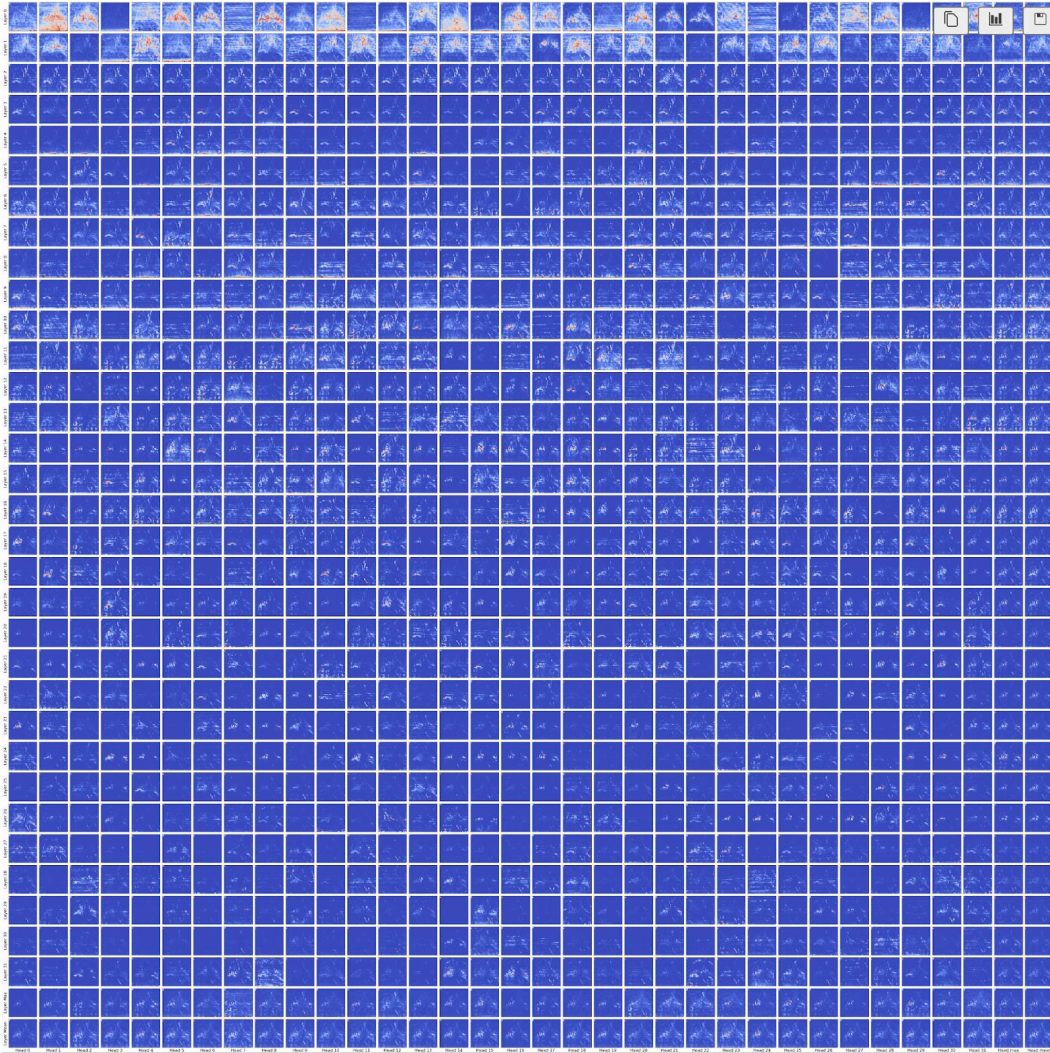


Supplementary Figure 4: Attention weights for the generated word **devices** from different layers and heads of the model.





Supplementary Figure 5: All attention weights for the generated word **aortic** from all layers and heads of the model.



Supplementary Figure 6: All attention weights for the generated word **opacifications** from all layers and heads of the model.

Model	Size	CheXbert								Rad-Graph	BLEU			ROUGE	
		("uncertain" as <i>negative</i> )				("uncertain" as <i>positive</i> )					F1	(1)	(4)		-L
		Micro-avg		Macro-avg		Micro-avg		Macro-avg							
		F1-14	F1-5	F1-14	F1-5	F1-14	F1-5	F1-14	F1-5						
LLaVA-Rad	7B	<b>57.3</b>	57.4	39.5	47.7	<b>57.3</b>	<b>60.2</b>	<b>44.0</b>	<b>53.3</b>	29.4	38.1	<b>15.4</b>	<b>30.6</b>		
Med-PaLM M	84B	53.6	<b>57.9</b>	<b>39.8</b>	<b>51.6</b>	-	-	-	-	26.7	32.3	11.3	27.3		
GPT-4V	-	35.5	25.8	20.4	19.6	35.6	33.3	25.3	29.6	13.2	16.4	1.9	13.2		
MAIRA-1	7B	55.7	56.0	38.6	47.7	55.3	58.8	42.3	51.7	<b>29.6</b>	39.2	14.2	28.9		
CheXagent	7B	39.3	41.2	24.7	34.5	39.4	42.1	27.3	35.8	20.5	16.9	4.7	21.5		
LLaVA-Med	7B	27.2	22.0	15.5	16.6	27.3	24.4	18.7	20.5	6.5	22.2	1.0	13.3		
LLaVA	7B	22.9	23.4	15.4	17.5	23.7	26.9	17.0	20.3	4.5	21.0	1.3	13.8		
Flamingo-CXR	<1B	-	-	-	-	51.9	56.5	-	-	20.5	-	10.1	29.7		
CvT2Dist.	<1B	44.2	-	30.7	-	-	-	-	-	-	<b>39.3</b>	12.7	28.6		
$\mathcal{M}^2$ trans	<1B	-	-	-	-	-	56.7	-	-	-	-	11.4	-		
RGRG	<1B	-	-	-	-	-	54.7	-	-	-	37.3	12.6	26.4		
R2Gen	<1B	-	-	-	-	22.8	34.6	-	-	-	35.3	8.6	27.7		
TieNet	<1B	-	-	-	-	-	27.1	-	-	-	-	8.1	-		

Supplementary Table 1: Evaluation results on the MIMIC-CXR test set. B denotes billions in the column of Size.

Model Version	CheXbert								Rad- Graph		BLEU		ROUGE -L
	("uncertain" as <i>negative</i> )				("uncertain" as <i>positive</i> )				F1	(1)	(4)		
	Micro-avg		Macro-avg		Micro-avg		Macro-avg						
	F1-14	F1-5	F1-14	F1-5	F1-14	F1-5	F1-14	F1-5	F1	(1)	(4)		
LLaVA-Rad	<b>57.3</b>	<b>57.4</b>	<b>39.5</b>	47.7	<b>57.3</b>	<b>60.2</b>	<b>44.0</b>	53.3	29.4	38.1	<b>15.4</b>	<b>30.6</b>	
Variant #1	55.5	55.2	38.4	46.9	55.9	58.4	42.5	51.1	29.6	<b>38.5</b>	<b>15.4</b>	<b>30.6</b>	
Variant #2	55.6	56.4	38.5	<b>48.6</b>	55.7	59.5	41.6	52.9	28.9	37.5	15.2	30.3	
Variant #3	55.7	56.2	39.1	47.4	55.8	59.0	43.1	51.4	<b>29.7</b>	37.9	15.6	31.0	
Variant #4	56.2	56.9	38.6	48.3	56.1	<b>60.2</b>	43.0	<b>54.0</b>	27.6	29.9	10.0	26.3	
Variant #5	50.6	53.3	30.7	42.7	49.2	54.1	33.6	45.0	25.0	16.9	5.0	16.4	
Variant #6	51.1	52.9	31.0	43.6	51.4	56.3	35.1	48.6	26.9	35.0	13.9	29.4	
Variant #7	49.8	52.1	30.5	42.4	50.3	55.4	34.5	48.0	26.5	34.4	13.7	29.1	
Variant #8	49.6	52.2	31.3	42.8	50.1	55.6	35.0	47.8	26.9	34.3	13.7	29.3	
Analysis #1	96.7	98.3	95.1	97.8	96.9	98.4	95.5	97.8	93.2	82.2	78.8	90.9	

**Stage 1** (*image encoder pre-training*) → **Stage 2** (*alignment*) → **Stage 3** (*fine-tuning*)

Variant #1: Stage 1 pre-trains the image encoder on MIMIC-CXR only. Stage 2&3 are the same.

Variant #2: No stage-1 pretraining. Stage 2&3 are the same.

Variant #3: Stage 1 is the same. Stage 2&3 only use rule-processed MIMIC-CXR training data.

Variant #4: Stage 1 is the same. Stage 2&3 only use GPT-4 processed MIMIC-CXR training data.

Variant #5: Stage 1&2 are the same. No stage 3.

Variant #6: No stage 1. Stage 2 initializes with LLaVA-v1.5 pre-trained weights.

Variant #7: No stage 1. Stage 2 initializes the image encoder with OpenAI CLIP pre-trained weights.

Variant #8: No stage 1. Stage 2 initializes the image encoder with BiomedCLIP pre-trained weights.

Analysis #1: Evaluate GPT-4 processed test data against rule-processed test data.

Supplementary Table 2: Ablation study.

MIMIC-CXR	Training	Validation	Test
Patients	63,169	487	289
Studies	213,365	1,733	3,041
DICOMs (AP/PA)	237,972	1,959	3,403
Rule-based reports	162,969	1,286	2,461
GPT-structured reports	237,073	1,952	-
Total data	400,042	3,238	2,461

Supplementary Table 3: Number of patients, studies and DICOMs in AP/PA views across official MIMIC-CXR splits. Numbers of image-text pairs generated by official rule-based method and augmented by GPT-4 in training and validation splits, excluding texts with no *Findings* extracted.

Dataset	Patients	Images	Label Types	Text Length			Pre-training Image-Text Pairs
				Min	Max	Avg.	
<i>Synthetic Findings</i>							
CheXpert [24]	64,540	224,316	14	3	89	27.8	190,999
BraX [41]	19,351	40,967	14	3	76	32.1	19,309
CandidPTX [14]	13,744	19,237	3	12	33	22.8	19,237
VinDR [37]	18,000	18,000	6	79	125	103.2	15,000
JF Healthcare [17]	10,000	10,000	1	4	12	7.6	10,000
<i>Real-World Findings</i>							
MIMIC-CXR [26]	65,379	377,095	–	3	183	85.1	353,350
PadChest [6]	67,625	168,861	–	1	133	12.5	89,540
Total:							697,435

Supplementary Table 4: An extensive collection of 697 thousand Chest X-ray datasets used for pre-training a domain-specific image encoder BiomedCLIP-CXR. MIMIC-CXR contains images with both frontal and lateral views, while others only include frontal views. *Synthetic Findings* are generated via template sentences derived from supervised clinical labels; *Real-World Findings* are extracted from patient reports utilizing GPT.

---

Positive <condition>:

1. The radiograph reveals evidence of <condition>.
2. The radiograph demonstrates areas consistent with <condition>.
3. There are findings suggestive of <condition>.
4. There is presence of <condition>.
5. There is a positive finding of <condition>.
6. The radiographic examination of the chest reveals the presence of <condition>.
7. There is evidence of <condition>.
8. <Condition> is present.

Negative <condition>:

1. No evidence of <condition> is observed.
2. <Condition> is not identified.
3. The radiograph does not show any signs of <condition>.
4. There is no indications of <condition> in the radiograph.
5. No <condition> is identified in the examined region.
6. No signs of <condition> is observed.
7. The image does not conclusively indicate <condition>.

Uncertain <condition>:

1. There is uncertainty regarding <condition>.
2. The presence of <condition> is uncertain based on the current examination.
3. The image shows uncertainty in <condition>.

No findings:

1. The radiographic examination of the chest reveals no significant abnormalities or pathologies.
2. The radiographic examination of the patient does not reveal any significant abnormal findings.

No support devices:

1. There is no evidence of any support devices in the chest area.
2. There are no support devices seen in the current study.
3. There are no support devices in place.

Pleural others:

1. There are some pleural abnormalities that do not fit into the common categories of pleural diseases.
2. Other pleural abnormalities are also observed.

No pleural others:

1. No other pleural abnormalities were detected in the radiograph.
2. There are no findings related to other pleural abnormalities.

Uncertain pleural others:

1. There are ambiguous findings related to the pleura.
  2. There is no visible pleural abnormality, although the image does not completely exclude all potential pleural conditions.
- 

Supplementary Table 5: Template sentences for deriving synthetic reports from supervised clinical conditions.

---

You are an expert medical assistant AI capable of modifying clinical documents to user specifications. You make minimal changes to the original document to satisfy user requests. You never add information that is not already directly stated in the original document.

Extract four sections from the input radiology report: 'Examination', 'Indication', 'Findings' and 'Impression'. Leave an extracted section as null if it does not exist in the original report. The output should be in JSON format. An Indication section can refer to the History, Indication or Reason for Study sections in the original report. Remove any information not directly observable from the current imaging study. For instance, remove any patient demographic data, past medical history, or comparison to prior images or studies. The generated 'Findings' and 'Impression' sections should not reference any changes based on prior images, studies, or external knowledge about the patient. Rewrite such comparisons as a status observation based only on the current image or study. Remember to remove any numbering or bullets.

Examples of inputs and expected outputs:

INPUT:

EXAMINATION: XR CHEST AP PORTABLE

INDICATION: Small right apical pneumothorax after lung biopsy.

FINDINGS: Single portable view of the chest was obtained. Copared with 10:42 AM. The small right apical pneumothorax has decreased slightly in size, the improvement best appreciated laterally where it now measures 10 mm compared to 14 mm before. At the lung apex it now measures 1.6 and compared to 2.1 cm previously. A subtle right apical pulmonary contusion is grossly stable. Minor chest wall emphysema along the right exilla has not changed significant delay. There is no metastatic shift. No pleural effusion is evident.

OUTPUT:

```
{"EXAMINATION": "XR CHEST AP PORTABLE.",  
"INDICATION": "Small right apical pneumothorax after lung biopsy.",  
"FINDINGS": "Single portable view of the chest was obtained. The small right apical  
pneumothorax measures 10mm. At the lung apex it measures 1.6cm. A subtle right apical  
pulmonary contusion is grossly stable. Minor chest wall emphysema is noted along the  
right exilla. There is no metastatic shift. No pleural effusion is evident.",  
"IMPRESSION": null}
```

---

Supplementary Table 6: GPT Prompt for report structuring.

Original	<p><b>INDICATION:</b> ___ year old woman with likely ileus after cystectomy // NGT placement confirmation NGT placement confirmation</p> <p><b>IMPRESSION:</b> No previous images. Nasogastric tube extends to the mid body of the stomach, be for coiling on itself so that the tip lies close to the esophagogastric junction. For more optimal positioning, the to would have to be pulled back almost 10 cm and then hopefully redirected toward the lower stomach. Cardiac silhouette is within normal limits and there is no vascular congestion, pleural effusion, or acute focal pneumonia.</p>
Rule-based	<p><b>INDICATION:</b> ___ year old woman with likely ileus after cystectomy // NGT placement confirmation NGT placement confirmation</p> <p><b>FINDINGS:</b> nan</p> <p><b>IMPRESSION:</b> No previous images. Nasogastric tube extends to the mid body of the stomach, be for coiling on itself so that the tip lies close to the esophagogastric junction. For more optimal positioning, the to would have to be pulled back almost 10 cm and then hopefully redirected toward the lower stomach. Cardiac silhouette is within normal limits and there is no vascular congestion, pleural effusion, or acute focal pneumonia.</p>
GPT-structured	<p><b>INDICATION:</b> ___ year old woman with likely ileus after cystectomy // NGT placement confirmation</p> <p><b>FINDINGS:</b> Nasogastric tube extends to the mid body of the stomach, before coiling on itself so that the tip lies close to the esophagogastric junction. Cardiac silhouette is within normal limits and there is no vascular congestion, pleural effusion, or acute focal pneumonia.</p> <p><b>IMPRESSION:</b> For more optimal positioning, the tube would have to be pulled back almost 10 cm and then hopefully redirected toward the lower stomach.</p>

Supplementary Table 7: Comparison between GPT-structured sections and rule-based extractions. GPT affixes broken words (in aquamarine), removes repeated phrases (in apricot) and references to prior images (in salmon), and arranges the text into appropriate *Findings* and *Impression* sections (in green yellow) without being constrained by the original section title.

Model	Key Training Data	Image Encoder	Key Evaluations
LLaVA	Image Captions + GPT4	CLIP	VQA, LLaVA-Bench
LLaVA-Med	PMC Captions + GPT4	BiomedCLIP	VQA, LLaVA-Bench
LLaVA-Rad	Radiology Data + GPT4	BiomedCLIP-CXR	CheXprompt/CheXpert

Supplementary Table 8: Evolution of the LLaVA model families for biomedical domains